

## Article

# Dynamic Response of an Elastic Tube-like Nanostructure Embedded in a Vibrating Medium and under the Action of Moving Nano-Objects

Xiaoxia Ma <sup>1</sup>, Mojtaba Roshan <sup>2</sup>, Keivan Kiani <sup>3,\*</sup> and Ali Nikkhoo <sup>4</sup><sup>1</sup> Department of Basic Courses, Jiaozuo University, Jiaozuo 454000, China<sup>2</sup> Department of Civil and Environmental Engineering, University of Massachusetts Dartmouth, Dartmouth, MA 02747, USA<sup>3</sup> Department of Civil Engineering, K.N. Toosi University of Technology, Valiasr Ave., P.O. Box 15875-4416, Tehran 1996715433, Iran<sup>4</sup> Department of Civil Engineering, University of Science and Culture (USC), Tehran 1461968151, Iran

\* Correspondence: k\_kiani@kntu.ac.ir or keivankiani@yahoo.com; Tel.: +98-21-88779473; Fax: +98-21-88779476

**Abstract:** In recent years, researchers have looked at how tube-like nanostructures respond to moving loads and masses. However, no one has explored the scenario of a nanostructure embedded in a vibrating medium used for moving nano-objects. In this study, the governing equations of the problem are methodically derived using the nonlocal elasticity of Eringen as well as the Rayleigh and Reddy–Bickford beam theories. Analytical and numerical solutions are developed for capturing the nonlocal dynamic deflection of the nanostructure based on the moving nanoforce approach (excluding the inertia effect) and the moving nanomass approach (including the inertia effect), respectively. The results predicted by the established models are successfully verified with those of other researchers in some special cases. The results reveal that for low velocities of the moving nano-object in the absence of the medium excitation, the midspan deflection of the simply supported nanotube exhibits an almost symmetric time-history curve; however, by increasing the nano-object velocity or the medium excitation amplitude, such symmetry is violated, mainly due to the lateral inertia of the moving nano-object, as displayed by the corresponding three-dimensional plots. The study addresses the effects of the mass and velocity of the moving nano-object, amplitude, and frequency of the medium excitation, and the lateral and rotational stiffness of the nearby medium in contact with the nanostructure on the maximum dynamic deflection. The achieved results underscore the significance of considering both the inertial effect of the moving nano-object and the shear effect of stocky nanotubes embedded in vibrating media. This research can serve as a strong basis for conducting further investigations into the vibrational properties of more intricate tube-shaped nanosystems that are embedded in a vibrating medium, with the aim of delivering nano-objects.

**Keywords:** dynamic response; vibrating surrounded medium; tube-like nanostructures; Rayleigh and Reddy–Bickford beam theories; nonlocal continuum mechanics; moving nano-object



**Citation:** Ma, X.; Roshan, M.; Kiani, K.; Nikkhoo, A. Dynamic Response of an Elastic Tube-like Nanostructure Embedded in a Vibrating Medium and under the Action of Moving Nano-Objects. *Symmetry* **2023**, *15*, 1827. <https://doi.org/10.3390/sym15101827>

Academic Editor: Christophe Humbert

Received: 7 August 2023

Revised: 8 September 2023

Accepted: 13 September 2023

Published: 26 September 2023



**Copyright:** © 2023 by the authors. Licensee MDPI, Basel, Switzerland. This article is an open access article distributed under the terms and conditions of the Creative Commons Attribution (CC BY) license (<https://creativecommons.org/licenses/by/4.0/>).

## 1. Introduction

Nanostructured materials are commonly defined as those materials whose structural elements (i.e., clusters, crystallites, or molecules) possess dimensions in the interval of 1–100 nm. They can be spherical, conical, spiral, cylindrical, tubular, flat, hollow, or irregular in shape and can be generally classified into four material-based categories, including organic, inorganic, composite, and carbon-based. Among these various types of nanostructures, tube-like nanostructures (one-dimensional nanomaterials), such as carbon nanotubes and boron-nitride nanotubes (CNTs and BNNTs), provide a suitable environment for translocating nano-objects (i.e., zeroth-order nanomaterials) and nanofluids due to their

brilliant geometrical, physical, and chemical properties [1–4]. For example, the frictionless nature, as well as the smoothness of the inner surface of the CNTs, offer them for fast transport of nanofluidic flows [5–9] and nano-objects (i.e., gene, molecule, and so on) [10–15], particularly for water molecules. For instance, an investigation showed that the roughness in the tube walls results in a robust hydrogen-bonding network, and no substantial flow enhancement would be attained in rough tubes [16]. In addition, extensive laboratory and theoretical research have been carried out on drug transport by CNTs since these brilliant nanostructures have the ability to cross the cell membrane and can transfer drugs to target cells in a harmless way without harming healthy cells [17]. Therefore, CNTs can be effectively utilized for the targeted and accurate delivery of drugs. Using this method increases the effectiveness of the treatment and reduces the side effects of drug use [18]. CNTs have the ability to be filled with metal oxide; these agents are suitable for MRI detection and the control of cancer cells [19]. Also, DNA molecules can be placed inside CNTs, which can be used in the fields of molecular sensors, electronic DNA sequencing, gene delivery, and DNA modulated molecular electronics [20]. There are two common methods for drug delivery by CNTs. In the first method, the drug is placed in the form of capsules inside the nanotube, and it is suitably shot towards the target cell; in the other method, the drug is attached to the surface of the nanotube and directed to the target cell [21]. The drug molecule can easily move from one side of the nanotube to its end, but due to the van der Waals force between the drug molecule and the inner surface of the nanotube, the molecule could not individually leave the nanotube [22], necessitating an appropriate externally driven agent. So far, various methodologies have been established to shoot (exit) the molecules from inside the nanotube, including the displacing approach [23]; temperature-driven pumping [24]; nanopumping [25]; the domino effect [26]; and electrical [13]. In most of the cases mentioned above, the tube-like nanostructure is embedded in a medium and used for the translocation of nano-objects. Due to the embedment state, any vibrations or excitations of the surrounding medium could influence the functionality and dynamic response of the CNT acted upon by moving nano-objects (MNOs); however, the theoretical aspects of such a crucial problem have been not thoroughly formulated.

Over the past two decades, the increased exploitation of nanotechnology and nanoscale materials has been accompanied by increased interest in nanomechanical simulations and the modeling of solids. Through nanoscale investigations, the discrepancy between experimental results and classical continuum mechanics (CCM) was revealed, proving that the CCM is not able to predict the results of our concern rationally since it does not consider small-scale parameters in its constitutive relations. With regard to this crucial deficiency of the CCM, several principal investigators proposed some size-dependent elasticity-based theories to accurately capture their responses, including the nonlocal elasticity theory of Eringen [27–31], the strain gradient theory of Mindlin [32,33], the nonlocal strain gradient theory (NSGET) of Lim et al. [34], the couple stress theory of Toupin [35,36], and the surface elasticity theory (SET) of Gurtin–Murdoch [37,38]. One of the most popular size-dependent theories is that established by Eringen, so-called nonlocal continuum mechanics (NCM), expressing that the stress field is naturally nonlocal, meaning that the stress field in a point also depends on the stresses of the nearby points (i.e., the nonlocality effect). Nonlocality is commonly incorporated into the constitutive relations through a specific factor, the so-called *small-scale parameter* (SSP), whose importance for each established nonlocal-based model can be determined by adjusting the resulting dispersion curves and those obtained from molecular dynamics [39–42]. The essential deficiency of the differential-based NCM (DBNCM) of Eringen is mostly related to the lack of prediction of the hardening behavior of solid structures at the nanoscale; however, in recent years, several investigations have proved that some paradoxical mechanical behaviors of structures modeled based on the above theory can be resolved by particular treatments, including through utilizing the integral-based NCM (IBNCM) of Eringen [43–45].

In the previous three decades, exploring the nanoengineering problems of nanostructures by employing the NCM, including free vibration [46–58], buckling and

postbuckling [59–64], sound wave propagation [65–70], and forced vibration [71–78], have been of great interest to interdisciplinary scholars. Perhaps this is due to the straightforwardness of the NCM in expressing the constitutive relations in solids; for example, in IBNCM, the nonlocal stress field is stated in terms of the local one by a simple expression as follows:  $\sigma_{mn}^{nl}(\mathbf{x}, t) = \int_{\Omega} \Lambda(|\mathbf{x} - \mathbf{y}|; l_s) \sigma_{mn}^l(\mathbf{y}, t) d\Omega$ , in which  $\Omega$  represents the total spatial domain of the nanostructure and  $d\Omega$  denotes a very tiny volume of this domain (where  $d\Omega = d\mathbf{y}$ ). Further,  $t$  is the time parameter;  $\sigma_{mn}^{nl} = \sigma_{mn}^{nl}(\mathbf{x}, t)$  and  $\sigma_{mn}^l = \sigma_{mn}^l(\mathbf{x}, t)$  are the nonlocal and local dynamical stress fields, respectively, where  $\mathbf{x} \in \Omega$  denotes the coordinates of a point in the spatial domain of the continuum-based nanostructure; and  $\Lambda = \Lambda(|\mathbf{x} - \mathbf{y}|; l_s)$  signifies the nonlocal kernel function that controls the influence domain of the nonlocal stress field through the level of  $l_s$ , namely, the small-scale parameter or SSF. Under certain conditions, as explained by Eringen in his book [31], this version of NCM could be reduced to DBNCM, as expressed by  $(1 - l_s^2 \nabla^2) \sigma_{ij}^{nl} = \sigma_{ij}^l$ , where  $\nabla$  is the nabla operator (i.e.,  $\partial^2[\cdot]/\partial x^2$ ,  $\partial^2[\cdot]/\partial x^2 + \partial^2[\cdot]/\partial y^2$ , and  $\partial^2[\cdot]/\partial x^2 + \partial^2[\cdot]/\partial y^2 + \partial^2[\cdot]/\partial z^2$ , respectively, for one-, two-, and three-dimensional domains), and  $(1 - l_s^2 \nabla^2)$  is commonly called the nonlocal operator. Another popular aspect of NCM is its broad applications to various unknown physical fields (i.e., thermal field, magnetic field, and so on), which are commonly governed by a single or a set of partial differential equations with their boundary conditions; however, the application of the above-introduced size-dependent theories is limited to solid structures. Under the umbrella of the above-mentioned two benefits, NCM has been of interest to applied mechanics communities in revealing the role of the nonlocality of the chemical/physical/mechanical behaviors of nanostructures, leading us to more rational prediction results.

It is worth noting that despite extensive applications of the SET and NSGET for studying the buckling and vibrations of microscale/nanoscale structures with flexural behavior in recent years, as evidenced by studies such as those given in Refs. [79–81], these advanced theories of continuum mechanics have rarely been adopted for mechanical analyses of SWCNTs. One possible explanation for this is that the surface effect is only significant in nanostructures consisting of multiple layers of atoms across their thickness, while SWCNTs are made by wrapping a single-layered graphene sheet, which makes the consideration of surface parameters somewhat irrational. Additionally, the NSGET typically employs two small-scale factors, namely, a nonlocal factor and a strain gradient factor, in its formulations, but the role of the strain gradient factor in the elastodynamic response resulting from the common forced vibrations of nanotubes is almost negligible. NCM has been commonly employed for various vibrational problems associated with CNTs, given these reasons.

Concerning the application of NCM to vibrations of nanostructures under the action of MNOs, some investigators, via beam models [82–96], studied their nonlocal vibrations. In most of these explorations, nonlocal beam models (i.e., Bernoulli-Euler, Rayleigh, or Timoshenko, Levinson, or Reddy (i.e., higher-order)) were utilized for establishing the nonlocal version of the governing equations of a single nanobeam or multiple-nanobeam-systems, and the roles of the main properties of the MNO (i.e., mass weight and velocity) and the geometrical characteristics of the nanobeam on the various dynamic responses of the nanobeam were displayed and discussed in some detail. In addition, nonlocal vibrations of two-dimensional structures (i.e., mostly nanoplates and nanoscaled platelets) in the presence of in-contact MNO have been of interest to scholars [97–102]. In all of these investigations (i.e., both one- and two-dimensional nanostructures acted upon by MNOs), the possible vibration of the surrounding environment of the nanostructure on its overall vibrations was excluded and thereby the simultaneous excitations of the nanobeam due to the both vibrating medium and MNO were not addressed. With regard to this lack of scientific rigour, the authors herein decided to methodically explore the problem to rationally respond to the above-raised crucial query.

Herein, some useful nonlocal models based on the Rayleigh and Reddy beam theories (NRABT and NREBT) are established to examine transverse vibrations of the nanotube (NT) embedded in a vibrating medium used for translocating nano-objects. After obtaining their nonlocal-based equations of motion and solving via the Galerkin-based modal approach and generalized Newmark- $\beta$  methodology, their nonlocal deflections were appropriately assessed. Afterward, the roles of the mass and velocity of the MNO, amplitude, and frequency of the vibrating medium, NT's length, nonlocality, and shear effect in the maximum deflections are comprehensively investigated and discussed. Special attention has been also devoted to both the shear and inertial effects, as crucial factors in the suitable mathematical modeling of the NT and MNO, respectively.

## 2. Description and Assumptions Used in the Proposed Models

As illustrated in Figure 1, an NT-like structure is affected by both a vibrating elastic medium and moving nanomass excitation. The NT has a length of  $l_b$  and an average radius of  $r_m$ . The harmonic elastic medium excitation is denoted by  $w_g(t) = a_g \sin(\bar{\omega}t)$ , where  $a_g$  and  $\bar{\omega}$  are the amplitude and frequency of the medium excitation, respectively. Additionally, an MNO with a mass  $M$  and a constant speed  $v$  passes through the NT, and its position at any moment can be represented by  $x_M = vt$ , indicating that the MNO was positioned at the left end at  $t = 0$ . The NT foundation is modeled using the Pasternak foundation model, with  $k_r$  and  $k_t$  representing the stiffness of the rotational and transverse springs, respectively. During the course of excitation of the nanotube by the MNO or vibrating elastic medium, the nanotube is fully in contact with the medium, which is modeled here by a two-parameter foundation model (i.e., the Pasternak foundation model, which is essentially characterized by two constants:  $k_r$  and  $k_t$ ). These factors mainly depend on the material properties of the elastic medium (i.e., Young's modulus, shear modulus, and Poisson's ratio), the existing bond between the nanotube and the surrounding elastic medium (mainly van der Waals (vdW) forces), as well as its geometrical properties (i.e., a characteristic length of the medium, for example, the depth of the nanofoundation, the depth of the embedment, and so on), and these are assumed to be constants during vibrations. Because dislocations and nanocracks have not developed within the medium, and the nanotube does not experience any mis-bonding at the interface (i.e., the so-called mechanically imperfect interface), the material properties of the elastic medium do not change/retained.

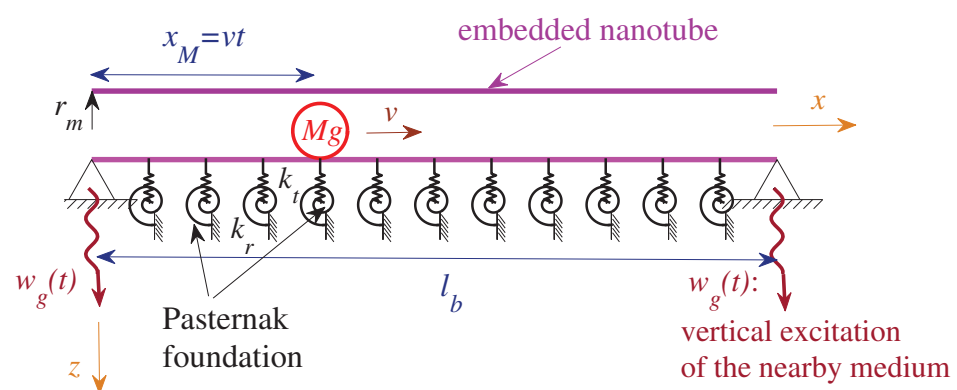


**Figure 1.** An embedded continuum-based tube-like nanostructure acted upon by the excitations of both elastic medium and MNO.

When it comes to studying MNO mechanical problems, there are two common approaches that could be considered: the moving nanoforce approach (MNFA) and the moving nanomass approach (MNMA). While the MNFA only takes into account the weight of nano-objects without considering transverse inertia, the MNMA includes nano-object inertial forces in the equations of motion for the rational prediction of transverse vibrations. However, it is important to note that both approaches used here ignore the friction force

between the MNO's outer surface and the NT's inner surface. Regardless of the MNO's speed, it is rationally assumed that the MNO remains in contact with the NT surface during the passage phase. This study aims to provide a comprehensive examination of how significant parameters affect NT vibrations, utilizing the NRABT and NREBT based on the MNFA and MNMA. For this purpose, the equations of motion are derived for each theory within the appropriate framework, presenting an analytical solution for the MNFA and an appropriate numerical method for the MNMA to analyze the problem for the major elastodynamic fields of the NT.

### 3. Investigating Vibrations under Excitations of Elastic Medium and MNO Based on the NRABT

#### 3.1. Nonlocally Developed Governing Equations

The equation of motion of transverse vibrations of a tube-like nanostructure under the action of a moving nano-object of weight  $Mg$  and excitation of the harmonic elastic environment of the form  $w_g(t) = a_g \sin(\bar{\omega}t)$  based on the NRABT can be stated as follows [50,83,103]:

$$\rho_b \left( A_b \frac{\partial^2 w_t^R}{\partial t^2} - I_b \frac{\partial^4 w_t^R}{\partial t^2 \partial x^2} \right) + k_t (w_t^R - w_g) - k_r \frac{\partial^2 w_t^R}{\partial x^2} - \frac{\partial^2 (M_b^{nl})^R}{\partial x^2} = f^R, \quad (1)$$

where  $t_f = l_b/v$  represents the time when the MNO leaves the NT,  $w^R$  denotes the pure dynamical deflection field of the NT,  $w_t^R$  is the total deflection field, and  $f^R = f^R(x, t)$  stands for the transverse dynamic loads that act on the beam-like nanostructure. In the above relationship,  $k_t$ ,  $k_r$ ,  $\rho_b$ ,  $A_b$ , and  $I_b$ , respectively, the stiffness of the translational spring, the stiffness of the torsional spring, density, the cross-sectional area, and the moment of inertia of the equivalent continuum structure (ECS), are associated with the NT.

For a moving nano-object of weight  $Mg$  at the longitudinal location of  $x_M$ , the concentrated force exerted on the NT accounting for the transverse inertia effect is stated as [84,104–106]:  $f^R(x, t) = M \left( g - \varkappa \frac{D^2 w_t^R}{Dt^2} \right) \delta(x - x_M) H(t_f - t)$ , in which  $M \frac{D^2 w_t^R}{Dt^2}$  signifies the total transverse inertia of the MNO;  $H$  and  $\delta$  represent Heaviside's function and Dirac's delta function, respectively; and  $\frac{D[\cdot]}{Dt}$  stands for the first material derivative of the field  $[\cdot]$  of the vibrating NT just at the MNO's location. The Heaviside's function is utilized to control the entry and exit of the MNO into the NT, whereas Dirac's delta function is employed for point load modeling of the MNO. In the above relationship,  $\varkappa$  is the representative of the chosen approach, and it could take the values 0 or 1, where 0 indicates the MNFA and 1 represents the MNMA. The expressions of the non-local bending moment  $((M_b^{nl})^R)$  and the total transverse displacement  $(w_t^R)$  of the NT modeled based on the NRABT are defined as follows:

$$\begin{aligned} w_t^R(x, t) &= w^R(x, t) + w_g(t), \\ \Lambda \left\{ (M_b^{nl})^R \right\} &= (M_b^l)^R = -E_b I_b \frac{\partial^2 w^R}{\partial x^2}, \end{aligned} \quad (2)$$

in which  $\Lambda[\cdot] = [\cdot] - (e_0 a)^2 \frac{\partial^2 [\cdot]}{\partial x^2}$  represents the non-local operator,  $e_0 a$  is the small-scale parameter, and  $E_b$  is Young's modulus of the ECS pertinent to the NT. By inserting the expression  $w_t^R$  and by applying the non-local operator on the sides of Equation (1), the non-local equations of motion in terms of the transverse displacement field are obtained:

$$\Lambda \left\{ \rho_b \left( A_b \frac{\partial^2 w^R}{\partial t^2} - I_b \frac{\partial^4 w^R}{\partial t^2 \partial x^2} \right) + k_t w^R - k_r \frac{\partial^2 w^R}{\partial x^2} \right\} + E_b I_b \frac{\partial^4 w^R}{\partial x^4} = \Lambda \left\{ M \left( g - \varkappa \frac{D^2 w^R}{Dt^2} \right) \delta(x - x_M) H(t_f - t) - \left[ \varkappa M \delta(x - x_M) H(t_f - t) + \rho_b A_b \right] \frac{d^2 w_g}{dt^2} \right\}, \tag{3}$$

by substituting  $w_g(t) = a_g \sin(\bar{\omega}t)$  in Equation (3), the following relation can be reached:

$$\Lambda \left\{ \rho_b \left( A_b \frac{\partial^2 w^R}{\partial t^2} - I_b \frac{\partial^4 w^R}{\partial t^2 \partial x^2} \right) + k_t w^R - k_r \frac{\partial^2 w^R}{\partial x^2} \right\} + E_b I_b \frac{\partial^4 w^R}{\partial x^4} = \Lambda \left\{ M \left( g - \varkappa \frac{D^2 w^R}{Dt^2} \right) \delta(x - x_M) H(t_f - t) + \left[ \varkappa M \delta(x - x_M) H(t_f - t) + \rho_b A_b \right] a_g \bar{\omega}^2 \sin(\bar{\omega}t) \right\}. \tag{4}$$

To solve the problem in a more general way, we should present the obtained nonlocal motion equations in a dimensionless form as follows:

$$\bar{\Lambda} \left\{ \frac{\partial^2 \bar{w}^R}{\partial \tau^2} - \lambda^{-2} \frac{\partial^4 \bar{w}^R}{\partial \tau^2 \partial \xi^2} + \bar{k}_t \bar{w}^R - \bar{k}_r \frac{\partial^2 \bar{w}^R}{\partial \xi^2} \right\} + \frac{\partial^4 \bar{w}^R}{\partial \xi^4} = \bar{\Lambda} \left\{ \bar{f}_M^R \left( 1 - \varkappa \frac{D^2 \bar{w}^R}{D\tau^2} \right) \delta(\xi - \xi_M) H(\tau_f^R - \tau) + \left[ \varkappa M_N \delta(\xi - \xi_M) H(\tau_f^R - \tau) + 1 \right] \bar{f}_g^R \sin(\bar{\Omega}^R \tau) \right\}, \tag{5}$$

where the dimensionless parameters are as follows:

$$\begin{aligned} \bar{w}^R &= \frac{w^R}{l_b}, \quad \xi = \frac{x}{l_b}, \quad \xi_M = \frac{x_M}{l_b}, \quad \bar{\Lambda} = [\cdot] - \mu^2 \frac{\partial^2 [\cdot]}{\partial \xi^2}, \quad \lambda = l_b \sqrt{\frac{A_b}{I_b}}, \quad \tau = \frac{t}{l_b^2} \sqrt{\frac{E_b I_b}{\rho_b A_b}}, \quad \bar{k}_t = \frac{k_t l_b^4}{E_b I_b}, \\ \bar{k}_r &= \frac{k_r l_b^2}{E_b I_b}, \quad \mu = \frac{e_0 a}{l_b}, \quad M_N = \frac{M}{\rho_b A_b l_b}, \quad \tau_f^R = \frac{1}{v l_b} \sqrt{\frac{E_b I_b}{\rho_b A_b}}, \quad \bar{f}_M^R = \frac{M g l_b^2}{E_b I_b}, \quad \bar{\Omega}^R = \bar{\omega} l_b^2 \sqrt{\frac{\rho_b A_b}{E_b I_b}}, \\ \bar{f}_g^R &= \frac{a_g}{l_b} (\bar{\Omega}^R)^2, \quad \frac{D^2 \bar{w}^R}{D\tau^2} = \left( \frac{E_b I_b}{\rho_b A_b g l_b^3} \right) \frac{\partial^2 \bar{w}^R}{\partial \tau^2} + 2 \left( \frac{v}{g l_b^2} \sqrt{\frac{E_b I_b}{\rho_b A_b}} \right) \frac{\partial^2 \bar{w}^R}{\partial \tau \partial \xi} + \left( \frac{v^2}{g l_b} \right) \frac{\partial^2 \bar{w}^R}{\partial \xi^2}. \end{aligned} \tag{6}$$

### 3.2. An Analytically Developed Solution Based on the MNFA ( $\varkappa = 0$ )

To discretize the dynamic deflection of the NT in the spatial domain, the modal analysis is utilized as  $\bar{w}^R(\xi, \tau) = \sum_{n=1}^{\infty} \bar{a}_n^R(\tau) \phi_n^w(\xi)$ , in which  $\phi_n^w$  represents the shape function of the  $n$ -th mode, where  $\phi_n^w(\xi) = \sin(n\pi\xi)$  is exploited for simply ended boundary conditions and  $\bar{a}_n^R(\tau)$  signifies the unknown time-dependent parameter. By putting this discretized version of the dimensionless deflection in the equation of motion given in Equation (5) under the condition  $\varkappa = 0$  (moving nanoforce approach), the following relationship can be reached:

$$\frac{\partial^2 \bar{a}_n^R}{\partial \tau^2} + \Gamma_n^2 \bar{a}_n^R = \beta_n^R \sin(g_n^R \tau) H(\tau_f^R - \tau) + \mathcal{A}_n^R \sin(\bar{\Omega}^R \tau), \tag{7}$$

where

$$\begin{aligned} \Gamma_n^2 &= \frac{(\bar{k}_t + \bar{k}_r (n\pi)^2) (1 + (n\pi\mu)^2) + (n\pi)^4}{(1 + (\frac{n\pi}{\lambda})^2) (1 + (n\pi\mu)^2)}, \quad \mathcal{A}_n^R = \frac{2\bar{f}_g^R (1 - \cos(n\pi))}{n\pi (1 + (\frac{n\pi}{\lambda})^2) (1 + (n\pi\mu)^2)}, \\ \beta_n^R &= \frac{2\bar{f}_M^R}{1 + (\frac{n\pi}{\lambda})^2}, \quad g_n^R = v_i n \pi l_b \sqrt{\frac{\rho_b A_b}{E_b I_b}}. \end{aligned} \tag{8}$$

According to the initial conditions of the governing equations of the problem, we have:

$$\bar{a}_n^R(0) = \frac{d\bar{a}_n^R}{d\tau}(0) = 0. \tag{9}$$

Using the Laplace transform, the unknown coefficients of the ordinary differential equation in Equation (8) can be obtained in the following form:

$$\mathcal{L}\{\bar{a}_n^R\} = \left( \frac{\beta_n^R g_n^R (1 - \cos(n\pi)) e^{-s\tau_f^R}}{(s^2 + \Gamma_n^2)(s^2 + (g_n^R)^2)} + \frac{\mathcal{A}_n^R \bar{\Omega}^R}{(s^2 + \Gamma_n^2)(s^2 + \bar{\Omega}^R{}^2)} \right). \tag{10}$$

By using the inverse Laplace transform, the unknown time coefficients can be obtained. According to the initial conditions given in Equation (9), the unknown displacement field of the problem can be calculated in the following form:

$$\bar{w}^R(\zeta, \tau) = \sum_{n=1}^{\infty} \left( \begin{aligned} &\mathcal{B}_n^R (g_n^R \sin(\Gamma_n \tau) - \Gamma_n \sin(g_n^R \tau)) - \\ &\mathcal{B}_n^R \cos(n\pi) \text{H}(\tau_f^R - 1) (g_n^R \sin(\Gamma_n(\tau - \tau_f^R)) - \Gamma_n \sin(g_n^R(\tau - \tau_f^R))) \\ &+ \mathcal{C}_n^R (\bar{\Omega}^R \sin(\Gamma_n \tau) - \Gamma_n \sin(\bar{\Omega}^R \tau)) \end{aligned} \right) \sin(n\pi\zeta), \tag{11}$$

in which,

$$\mathcal{B}_n^R = \frac{\beta_n^R}{\Gamma_n((g_n^R)^2 - \Gamma_n^2)}, \quad \mathcal{C}_n^R = \frac{\mathcal{A}_n^R}{\Gamma_n((\bar{\Omega}^R)^2 - \Gamma_n^2)}. \tag{12}$$

### 3.3. A Numerically Developed Solution Based on the MNMA ( $\varkappa = 1$ )

The Galerkin methodology on the basis of the modal analysis is employed to determine the dynamic response of nanotubes. For this purpose, by multiplying both sides of Equation (5) by  $\delta\bar{w}^R$  ( $\delta$  is the variational sign) and integrating over the length of the NT, the following can be written:

$$\begin{aligned} &\int_0^1 \left\{ \begin{aligned} &\delta\bar{w}^R \frac{\partial^2 \bar{w}^R}{\partial \tau^2} - \mu^2 \frac{\partial^2 (\delta\bar{w}^R)}{\partial \xi^2} \frac{\partial^2 \bar{w}^R}{\partial \tau^2} + \lambda^{-2} \frac{\partial (\delta\bar{w}^R)}{\partial \xi} \frac{\partial^3 \bar{w}^R}{\partial \tau^2 \partial \xi} + \mu^2 \lambda^{-2} \frac{\partial^2 (\delta\bar{w}^R)}{\partial \xi^2} \frac{\partial^4 \bar{w}^R}{\partial \tau^2 \partial \xi^2} + \\ &\bar{k}_t^R \bar{w}^R d\bar{w}^R - \mu^2 \bar{k}_t^R \bar{w}^R \frac{\partial^2 (\delta\bar{w}^R)}{\partial \xi^2} - \bar{k}_r^R \frac{\partial^2 \bar{w}^R}{\partial \xi^2} \delta\bar{w}^R + \mu^2 \bar{k}_r^R \frac{\partial^2 \bar{w}^R}{\partial \xi^2} \frac{\partial^2 (\delta\bar{w}^R)}{\partial \xi^2} + \frac{\partial^2 (\delta\bar{w}^R)}{\partial \xi^2} \frac{\partial^2 \bar{w}^R}{\partial \xi^2} \end{aligned} \right\} \text{ffi}\zeta \\ &= \int_0^1 \left\{ \begin{aligned} &(\delta\bar{w}^R - \mu^2 \frac{\partial^2 (\delta\bar{w}^R)}{\partial \xi^2}) \bar{f}_M^R (1 - \varkappa \frac{D^2 \bar{w}^R}{D\tau^2}) \delta(\zeta - \zeta_M) \text{H}(\tau_f^R - \tau) \\ &+ \delta\bar{w}^R [M_N \delta(\zeta - \zeta_M) \text{H}(\tau_f^R - \tau) + 1] \bar{f}_g^R \sin(\bar{\Omega}^R \tau) \end{aligned} \right\} d\zeta. \end{aligned} \tag{13}$$

After placing the discrete displacement field  $\bar{w}^R(\zeta, \tau) = \sum_{n=1}^{\infty} \bar{a}_n^R(\tau) \phi_n^{\bar{w}^R}(\zeta)$  in Equation (13) and sorting the relations obtained, the following second-order ODEs can be reached:

$$[\bar{\mathbf{M}}_b^R]_{ij}^{ww} \frac{d^2 \bar{\mathbf{a}}_n^R}{d\tau^2} + [\bar{\mathbf{C}}_b^R]_{ij}^{ww} \frac{d \bar{\mathbf{a}}_n^R}{d\tau} + [\bar{\mathbf{K}}_b^R]_{ij}^{ww} \bar{\mathbf{a}}_n^R = \{\bar{\mathbf{f}}_b^R\}_i^w, \tag{14}$$

that the matrices of mass, damping, stiffness, and force are defined as follows:

$$[\bar{\mathbf{M}}_b^R]_{ij}^{ww} = 0.5(Y_{ij} + G_{ij}\lambda^{-2} + G_{ij}\mu^2 + (G_{ij}\mu)^2\lambda^{-2}) + M_N(1 + (i\pi\mu)^2) \sin(i\pi\zeta_M) \sin(j\pi\zeta_M) \text{H}(\tau_f^R - \tau), \tag{15}$$

$$[\bar{\mathbf{C}}_b^R]_{ij}^{ww} = 2\lambda\beta^R M_N j\pi (1 + (i\pi\mu)^2) \sin(i\pi\zeta_M) \cos(j\pi\zeta_M) \text{H}(\tau_f^R - \tau), \tag{16}$$

$$\begin{aligned} \left[\bar{\mathbf{K}}_b^R\right]_{ij}^{ww} = & 0.5G_{ij}^2 + 0.5\left(\bar{k}_t^R + \bar{k}_r^R(i\pi)^2\right)\left(Y_{ij} + G_{ij}\mu^2\right) - \\ & M_N\left(j\pi\lambda\beta^R\right)^2\left(1 + (i\pi\mu)^2\right)\sin(i\pi\xi_M)\sin(j\pi\xi_M)\text{H}\left(\tau_f^R - \tau\right), \end{aligned} \tag{17}$$

$$\begin{aligned} \left\{\bar{\mathbf{f}}_b^R\right\}_i^w = & M_N\left(\lambda\gamma^R\right)^2\left(1 + (i\pi\mu)^2\right)\sin(i\pi\xi_M)\text{H}\left(\tau_f^R - \tau\right) + \\ & \left(M_N\sin(i\pi\xi_M)\text{H}\left(\tau_f^R - \tau\right) + \frac{1 - \cos(i\pi)}{i\pi}\right)\bar{f}_s^R\sin(\bar{\Omega}^R\tau), \end{aligned} \tag{18}$$

where the parameters used in these equations are defined as follows:

$$Y_{ij} = \delta_{ij}, \quad G_{ij} = ij\pi^2\delta_{ij}, \quad C_l^R = \sqrt{\frac{E_{b1}}{\rho_{b1}}}, \quad \gamma^R = \frac{\sqrt{g_{l_b}^R}}{C_l^R}, \quad \beta^R = \frac{v}{C_l^R}, \tag{19}$$

where  $\delta_{ij}$  signifies the Kronecker delta tensor. Considering that the mass, damping, and stiffness matrices in the moving mass approach are time-dependent, the generalized Newmark- $\beta$  approach [107] is employed to determine the elastodynamic fields of the beam-like nanostructure under the effect of moving nano-objects.

#### 4. Investigating Vibrations under Excitations of Elastic Medium and MNO Based on the NREBT

##### 4.1. Nonlocally Developed Governing Equations

The nonlocal equations of motion of transverse vibrations of the NT under the action of elastic medium stimulation and MNO weight ( $Mg$ ) based on the higher-order shear beam theory are expressed as follows [50,103]:

$$I_0\frac{\partial^2 w_t^H}{\partial t^2} - \left(\alpha^2 I_6 - \alpha I_4\right)\frac{\partial^3 \psi^H}{\partial t^2 \partial x} - \alpha^2 I_6\frac{\partial^4 w_t^H}{\partial t^2 \partial x^2} - \frac{\partial\left(Q_b^{nl}\right)^H}{\partial x} + k_t\left(w_t^H - w_g\right) - \alpha\frac{\partial^2\left(P_b^{nl}\right)^H}{\partial x^2} = f^H, \tag{20}$$

$$\left(I_2 + \alpha^2 I_6 - 2\alpha I_4\right)\frac{\partial^2 \psi^H}{\partial t^2} + \left(\alpha^2 I_6 - \alpha I_4\right)\frac{\partial^3 w_t^H}{\partial t^2 \partial x} + \left(Q_b^{nl}\right)^H + \alpha\frac{\partial\left(P_b^{nl}\right)^H}{\partial x} - \frac{\partial\left(M_b^{nl}\right)^H}{\partial x} + k_r\psi^H = 0, \tag{21}$$

where  $w_t^H$  and  $\psi^H$  represent the total transverse displacement and the rotation angle of the ECS associated with the NT, respectively, and  $f^H = f^H(x, t)$  denotes the exerted transverse force on the NT due to the presence of the MNO inside the pore. Herein, this pointed load is considered in the following form [84]:  $f^H(x, t) = M\left(g - \varkappa\frac{D^2 w_t^H}{Dt^2}\right)\delta(x - x_M)\text{H}(t_f - t)$ . The shear force and bending moment of the NT based on the higher-order shear beam theory, in the framework of Eringen’s nonlocal continuum-based theory, are expressed as follows:

$$w_t^H(x, t) = w^H(x, t) + w_g(t), \tag{22}$$

$$\Lambda\left\{\left(Q_b^{nl}\right)^H\right\} = \left(Q_b^l\right)^H = k\left(\psi^H + \frac{\partial w^H}{\partial x}\right), \tag{23}$$

$$\Lambda\left\{\left(P_b^{nl}\right)^H\right\} = \left(P_b^l\right)^H = J_4\frac{\partial \psi^H}{\partial x} - \alpha J_6\left(\frac{\partial \psi^H}{\partial x} + \frac{\partial^2 w^H}{\partial x^2}\right), \tag{24}$$

$$\Lambda\left\{\left(M_b^{nl}\right)^H\right\} = \left(M_b^l\right)^H = J_2\frac{\partial \psi^H}{\partial x} - \alpha J_4\left(\frac{\partial \psi^H}{\partial x} + \frac{\partial^2 w^H}{\partial x^2}\right), \tag{25}$$

where

$$\Lambda[.] = [.] - (e_0 a)^2 [.]_{,xx}, \quad w_g(t) = a_g \sin(\bar{\omega}t), \quad \alpha_i = \frac{1}{3r_0^2}, \tag{26}$$

$$k = \int_{A_b} G_b (1 - 3\alpha z^2) dA, \quad I_m = \int_{A_b} \rho_b z^m dA; m = 0, 2, 4, 6, \quad J_n = \int_{A_b} E_b z^n dA; n = 2, 4, 6,$$

in which  $G_b$  denotes the shear modulus of the ECS. By applying the operator  $\Lambda$  to Equations (20) and (21) and then introducing Equations (22)–(25), the resulting relations and the nonlocal equations of motion are obtained in terms of nanosystem deformation fields:

$$\Lambda \left\{ I_0 \frac{\partial^2 w^H}{\partial t^2} - (\alpha^2 I_6 - \alpha I_4) \frac{\partial^3 \psi^H}{\partial t^2 \partial x} - \alpha^2 I_6 \frac{\partial^4 w^H}{\partial t^2 \partial x^2} + k_t w^H \right\} - k \left( \frac{\partial \psi^H}{\partial x} + \frac{\partial^2 w^H}{\partial x^2} \right) - \alpha J_4 \frac{\partial^3 \psi^H}{\partial x^3} + \alpha^2 J_6 \left( \frac{\partial^3 \psi^H}{\partial x^3} + \frac{\partial^4 w^H}{\partial x^4} \right) = \Lambda \left\{ \begin{aligned} &M \left( g - \varkappa \frac{D^2 w^H}{Dt^2} \right) \delta(x - x_M) H(t_f - t) - \\ &(\varkappa M \delta(x - x_M) H(t_f - t) + I_0) \frac{d^2 w_g}{dt^2} \end{aligned} \right\}, \tag{27}$$

$$\Lambda \left\{ (I_2 + \alpha^2 I_6 - 2\alpha I_4) \frac{\partial^2 \psi^H}{\partial t^2} + (\alpha^2 I_6 - \alpha I_4) \frac{\partial^3 w^H}{\partial t^2 \partial x} + k_r \psi^H \right\} + k \left( \psi^H + \frac{\partial w^H}{\partial x} \right) - (J_2 - 2\alpha J_4 + \alpha^2 J_6) \frac{\partial^2 \psi^H}{\partial x^2} - (\alpha^2 J_6 - 2\alpha J_4) \frac{\partial^3 w^H}{\partial x^3} = 0. \tag{28}$$

By inserting  $w_g(t) = a_g \sin(\bar{\omega}t)$  into the equations of motion given in Equations (27) and (28), the resulting relations can be rewritten as follows:

$$\Lambda \left\{ I_0 \frac{\partial^2 w^H}{\partial t^2} - (\alpha^2 I_6 - \alpha I_4) \frac{\partial^3 \psi^H}{\partial t^2 \partial x} - \alpha^2 I_6 \frac{\partial^4 w^H}{\partial t^2 \partial x^2} + k_t w^H \right\} - k \left( \frac{\partial \psi^H}{\partial x} + \frac{\partial^2 w^H}{\partial x^2} \right) - \alpha J_4 \frac{\partial^3 \psi^H}{\partial x^3} + \alpha^2 J_6 \left( \frac{\partial^3 \psi^H}{\partial x^3} + \frac{\partial^4 w^H}{\partial x^4} \right) = \Lambda \left\{ \begin{aligned} &M \left( g - \varkappa \frac{D^2 w^H}{Dt^2} \right) \delta(x - x_m) H(t_f - t) + \\ &(\varkappa M \delta(x - x_M) H(t_f - t) + I_0) a_g \bar{\omega}^2 \sin(\bar{\omega}t) \end{aligned} \right\}, \tag{29}$$

$$\Lambda \left\{ (I_2 + \alpha^2 I_6 - 2\alpha I_4) \frac{\partial^2 \psi^H}{\partial t^2} + (\alpha^2 I_6 - \alpha I_4) \frac{\partial^3 w^H}{\partial t^2 \partial x} + k_r \psi^H \right\} + k \left( \psi^H + \frac{\partial w^H}{\partial x} \right) - (J_2 - 2\alpha J_4 + \alpha^2 J_6) \frac{\partial^2 \psi^H}{\partial x^2} - (\alpha^2 J_6 - 2\alpha J_4) \frac{\partial^3 w^H}{\partial x^3} = 0. \tag{30}$$

In order to arrive at the dimensionless equations of motions, the following dimensionless parameters are defined:

$$\begin{aligned} w^H &= \frac{w^H}{l_b}, \quad \bar{\psi}^H = \psi^H, \quad \xi = \frac{x}{l_b}, \quad \tau = \frac{\alpha}{l_b^2} \sqrt{\frac{J_6}{I_0}} t, \quad \gamma_1^2 = \frac{\alpha I_4 - \alpha^2 I_6}{I_0 l_b^2}, \quad \gamma_2^2 = \frac{\alpha^2 I_6}{I_0 l_b^2}, \\ \gamma_3^2 &= \frac{k l_b^2}{\alpha^2 J_6}, \quad \gamma_4^2 = \frac{\alpha J_4 - \alpha^2 J_6}{\alpha^2 J_6}, \quad \gamma_6^2 = \frac{\alpha I_4 - \alpha^2 I_6}{I_2 - 2\alpha I_4 + \alpha^2 I_6}, \quad \gamma_7^2 = \frac{k I_0 l_b^4}{\alpha^2 J_6 (I_2 - 2\alpha I_4 + \alpha^2 I_6)}, \\ \gamma_8^2 &= \frac{(J_2 - 2\alpha J_4 + \alpha^2 J_6) I_0 l_b^2}{\alpha^2 J_6 (I_2 - 2\alpha I_4 + \alpha^2 I_6)}, \quad \gamma_9^2 = \frac{(\alpha J_4 - \alpha^2 J_6) I_0 l_b^2}{\alpha^2 J_6 (I_2 - 2\alpha I_4 + \alpha^2 I_6)}, \quad \bar{f}_M^H = \frac{M g l_b^2}{\alpha^2 J_6}, \quad \bar{f}_g^H = \frac{a_g}{l_b} \bar{\Omega}^2, \\ \bar{\Omega} &= \frac{\bar{\omega} l_b^2}{\alpha} \sqrt{\frac{I_0}{J_6}}, \quad \tau_f^H = \frac{\alpha}{v l_b} \sqrt{\frac{J_6}{I_0}}, \quad \xi = \frac{x_M}{l_b}, \quad M_N = \frac{M}{\rho_b A_b l_b}, \quad \bar{k}_r^H = \frac{k_r I_0 l_b^4}{\alpha^2 J_6 (I_2 - 2\alpha I_4 + \alpha^2 I_6)}, \\ \bar{k}_t^H &= \frac{k_t l_b^4}{\alpha^2 J_6}, \quad \frac{D^2 \bar{w}^H}{Dt^2} = \left( \frac{\alpha^2 J_6}{I_0 g l_b^3} \right) \frac{\partial^2 \bar{w}^H}{\partial \tau^2} + 2 \left( \frac{v \alpha}{g l_b^2} \sqrt{\frac{J_6}{I_0}} \right) \frac{\partial^2 \bar{w}^H}{\partial \tau \partial \xi} + \left( \frac{v^2}{g l_b} \right) \frac{\partial^2 \bar{w}^H}{\partial \xi^2}. \end{aligned} \tag{31}$$

By introducing the dimensionless parameters in Equation (31) to the equations of motion (29) and (30), the dimensionless governing equations are obtained as:

$$\bar{\Lambda} \left\{ \frac{\partial^2 \bar{w}^H}{\partial \tau^2} + \gamma_1^2 \frac{\partial^3 \bar{\psi}^H}{\partial \tau^2 \partial \xi} - \gamma_2^2 \frac{\partial^4 \bar{w}^H}{\partial \tau^2 \partial \xi^2} + \bar{k}_i^H \bar{w}^H \right\} - \gamma_3^2 \left( \frac{\partial \bar{\psi}^H}{\partial \xi} + \frac{\partial^2 \bar{w}^H}{\partial \xi^2} \right) - \gamma_4^2 \frac{\partial^3 \bar{\psi}^H}{\partial \xi^3} + \frac{\partial^4 \bar{w}^H}{\partial \xi^4} = \bar{\Lambda} \left\{ \bar{f}_m^H \left( 1 - \varkappa \frac{D^2 \bar{w}^H}{D\tau^2} \right) \delta(\xi - \xi_M) H(\tau_f^H - \tau) + \left( \varkappa M_N \delta(\xi - \xi_M) H(\tau_f^H - \tau) + 1 \right) \bar{f}_g^H \sin(\bar{\Omega}^H \tau) \right\}, \tag{32}$$

$$\bar{\Lambda} \left\{ \frac{\partial^2 \bar{\psi}^H}{\partial \tau^2} - \gamma_6^2 \frac{\partial^3 \bar{w}^H}{\partial \tau^2 \partial \xi} + \bar{k}_r^H \bar{\psi}^H \right\} + \gamma_7^2 \left( \bar{\psi}^H + \frac{\partial \bar{w}^H}{\partial \xi} \right) - \gamma_8^2 \frac{\partial^2 \bar{\psi}^H}{\partial \xi^2} + \gamma_9^2 \frac{\partial^3 \bar{w}^H}{\partial \xi^3} = 0. \tag{33}$$

4.2. An Analytically Developed Solution Based on the MNFA ( $\varkappa = 0$ )

To determine the dynamic response of the NT in the presence of simultaneous actions of the MNO and medium excitations, the modal analysis is implemented. To this end, we will discretize the unknown displacement field of the problem as  $\bar{w}^H(\xi, \tau) = \sum_{n=1}^{\infty} \bar{a}_n^H(\tau) \phi_n^W(\xi)$  and  $\bar{\psi}^H(\xi, \tau) = \sum_{n=1}^{\infty} \bar{b}_n^H(\tau) \phi_n^\psi(\xi)$ , in which  $\phi_n^{w_i}$  and  $\phi_n^{\psi_i}$ , respectively, represent the shape function corresponding to the transverse deformation and the rotation angle of the  $n$ -th vibration mode of the NT. For the nanostructure with simply supported ends,  $\phi_n^w(\xi) = \sin(n\pi\xi)$  and  $\phi_n^\psi(\xi) = \cos(n\pi\xi)$  are used. By replacing the above discrete forms in the dimensionless nonlocal motion relations, as provided in Equations (32) and (33), the following system of equations is obtained:

$$\begin{bmatrix} \zeta_{1n} & \zeta_{2n} \\ \zeta_{2n} & \zeta_{3n} \end{bmatrix} \begin{Bmatrix} \frac{\partial^2 \bar{a}_n^H}{\partial \tau^2} \\ \frac{\partial^2 \bar{b}_n^H}{\partial \tau^2} \end{Bmatrix} + \begin{bmatrix} \eta_{1n} & \eta_{2n} \\ \eta_{3n} & \eta_{4n} \end{bmatrix} \begin{Bmatrix} \bar{a}_n^H \\ \bar{b}_n^H \end{Bmatrix} = \begin{Bmatrix} \beta_n^H \sin(g_n^H \tau) H(\tau_f^H - \tau) + \mathcal{A}_n^H \sin(\bar{\Omega}^H \tau) \\ 0 \end{Bmatrix}, \tag{34}$$

that the initial conditions of this system of 2nd-order ODEs are given by:

$$\left\{ \bar{a}_n^H(0), \bar{b}_n^H(0) \right\} = \left\{ \frac{d\bar{a}_n^H}{d\tau}(0), \frac{d\bar{b}_n^H}{d\tau}(0) \right\} = \{0, 0\}, \tag{35}$$

where the dimensionless coefficients used in Equation (34) are defined as follows:

$$\begin{aligned} \eta_{1n} &= \bar{k}_i^H \left( 1 + (n\pi\mu)^2 \right) + \gamma_3^2 (n\pi)^2 + (n\pi)^4, & \eta_{2n} &= \gamma_3^2 n\pi - \gamma_4^2 (n\pi)^3, \\ \eta_{3n} &= \gamma_7^2 n\pi - \gamma_9^2 (n\pi)^3, & \eta_{4n} &= \bar{k}_r^H \left( 1 + (n\pi\mu)^2 \right) + \gamma_7^2 n\pi + \gamma_8^2 (n\pi)^2, \\ \zeta_{1n} &= \left( 1 + (n\pi\mu)^2 \right) \left( 1 + (n\pi\gamma_2)^2 \right), & \zeta_{2n} &= -\gamma_1^2 \left( (n\pi) + \mu^2 (n\pi)^3 \right), \\ \zeta_{3n} &= -\gamma_6^2 \left( (n\pi) + \mu (n\pi)^3 \right), & \zeta_{4n} &= 1 + (n\pi\mu)^2, & \mathcal{A}_n^H &= \frac{2\bar{f}_g^H}{n\pi} (1 - \cos(n\pi)) \end{aligned} \tag{36}$$

$$g_n^H = \frac{vn\pi l_b}{\alpha} \sqrt{\frac{I_0}{J_6}}, \quad \beta_n^H = 2\bar{f}_M^H \left( 1 + (n\pi\mu)^2 \right).$$

By applying the Laplace transform to the set of relations in Equation (34), it is obtainable:

$$\begin{aligned} \mathcal{L}\{\bar{a}_n^H\} &= \left( \frac{\beta_n^H g_n^H (1 - \cos(n\pi) e^{-s\tau_f^H}) (\zeta_{4n} s^2 + \eta_{4n})}{\Delta_n^H(s) (s^2 + (g_n^H)^2)} + \frac{\mathcal{A}_n^H \bar{\Omega}^H (\zeta_{4n} s^2 + \eta_{4n})}{\Delta_n^H(s) (s^2 + (\bar{\Omega}^H)^2)} \right), \\ \mathcal{L}\{\bar{b}_n^H\} &= - \left( \frac{\beta_n^H g_n^H (1 - \cos(n\pi) e^{-s\tau_f^H}) (\zeta_{3n} s^2 + \eta_{3n})}{\Delta_n^H(s) (s^2 + (g_n^H)^2)} + \frac{\mathcal{A}_n^H \bar{\Omega}^H (\zeta_{3n} s^2 + \eta_{3n})}{\Delta_n^H(s) (s^2 + (\bar{\Omega}^H)^2)} \right), \\ \Delta_n^H(s) &= (\zeta_{1n} \zeta_{4n} - \zeta_{2n} \zeta_{3n}) (s^2 + (r_{1n}^H)^2) (s^2 + (r_{2n}^H)^2), \end{aligned} \tag{37}$$

so that,

$$\begin{aligned} (r_{1n}^H)^2 &= \frac{(\zeta_{1n} \eta_{4n} + \zeta_{4n} \eta_{1n} - \zeta_{2n} \eta_{3n} - \zeta_{3n} \eta_{2n}) - \sqrt{\chi_n}}{2(\zeta_{1n} \zeta_{4n} - \zeta_{2n} \zeta_{3n})}, \\ (r_{2n}^H)^2 &= \frac{(\zeta_{1n} \eta_{4n} + \zeta_{4n} \eta_{1n} - \zeta_{2n} \eta_{3n} - \zeta_{3n} \eta_{2n}) + \sqrt{\chi_n}}{2(\zeta_{1n} \zeta_{4n} - \zeta_{2n} \zeta_{3n})}, \\ \chi_n &= (\zeta_{1n} \eta_{4n} + \zeta_{4n} \eta_{1n} - \zeta_{2n} \eta_{3n} - \zeta_{3n} \eta_{2n})^2 - 4(\eta_{1n} \eta_{4n} - \eta_{2n} \eta_{3n})(\zeta_{1n} \zeta_{4n} - \zeta_{2n} \zeta_{3n}). \end{aligned} \tag{38}$$

Using the inverse Laplace transform, the unknown coefficients of Equation (37) are obtained. By determining these coefficients, the dimensionless deformation fields of the NT under the effect of the MNO based on the MNFA-NREBM are obtained:

$$\bar{w}^H(\zeta, \tau) = \sum_{n=1}^{\infty} \left( \begin{aligned} &\frac{A_{1n}^H}{r_{1n}^H} \sin(r_{1n}^H \tau) + \frac{A_{2n}^H}{r_{2n}^H} \sin(r_{2n}^H \tau) + \frac{A_{3n}^H}{g_n^H} \sin(g_n^H \tau) - \cos(n\pi) H(\tau_f^H - 1) \times \\ &\left( \frac{A_{1n}^H}{r_{1n}^H} \sin(r_{1n}^H (\tau - \tau_f^H)) + \frac{A_{2n}^H}{r_{2n}^H} \sin(r_{2n}^H (\tau - \tau_f^H)) + \frac{A_{3n}^H}{g_n^H} \sin(g_n^H (\tau - \tau_f^H)) \right) \\ &+ \frac{B_{1n}^H}{r_{1n}^H} \sin(r_{1n}^H \tau) + \frac{B_{2n}^H}{r_{2n}^H} \sin(r_{2n}^H \tau) + \frac{B_{3n}^H}{\bar{\Omega}^H} \sin(\bar{\Omega}^H \tau) \end{aligned} \right) \sin(n\pi\zeta), \tag{39}$$

$$\bar{\psi}^H(\zeta, \tau) = \sum_{n=1}^{\infty} \left( \begin{aligned} &\frac{C_{1n}^H}{r_{1n}^H} \sin(r_{1n}^H \tau) + \frac{C_{2n}^H}{r_{2n}^H} \sin(r_{2n}^H \tau) + \frac{C_{3n}^H}{g_n^H} \sin(g_n^H \tau) - \cos(n\pi) H(\tau_f^H - 1) \times \\ &\left( \frac{C_{1n}^H}{r_{1n}^H} \sin(r_{1n}^H (\tau - \tau_f^H)) + \frac{C_{2n}^H}{r_{2n}^H} \sin(r_{2n}^H (\tau - \tau_f^H)) + \frac{C_{3n}^H}{g_n^H} \sin(g_n^H (\tau - \tau_f^H)) \right) \\ &+ \frac{D_{1n}^H}{r_{1n}^H} \sin(r_{1n}^H \tau) + \frac{D_{2n}^H}{r_{2n}^H} \sin(r_{2n}^H \tau) + \frac{D_{3n}^H}{\bar{\Omega}^H} \sin(\bar{\Omega}^H \tau) \end{aligned} \right) \cos(n\pi\zeta), \tag{40}$$

where

$$\begin{aligned}
 A_{1n}^H &= \frac{C_n^H (-\zeta_{4n}(r_{1n}^H)^2 + \eta_{4n})}{\left((r_{2n}^H)^2 - (r_{1n}^H)^2\right)\left((g_n^H)^2 - (r_{1n}^H)^2\right)}, & A_{2n}^H &= \frac{C_n^H (-\zeta_{4n}(r_{2n}^H)^2 + \eta_{4n})}{\left((r_{1n}^H)^2 - (r_{2n}^H)^2\right)\left((g_n^H)^2 - (r_{2n}^H)^2\right)} \\
 A_{3n}^H &= \frac{C_n^H (-\zeta_{4n}(g_n^H)^2 + \eta_{4n})}{\left((r_{1n}^H)^2 - (g_n^H)^2\right)\left((r_{2n}^H)^2 - (g_n^H)^2\right)}, & B_{1n}^H &= \frac{\mathfrak{D}_n^H (-\zeta_{4n}(r_{1n}^H)^2 + \eta_{4n})}{\left((r_{2n}^H)^2 - (r_{1n}^H)^2\right)\left((\bar{\Omega}^H)^2 - (r_{1n}^H)^2\right)}, \\
 B_{2n}^H &= \frac{\mathfrak{D}_n^H (-\zeta_{4n}(r_{2n}^H)^2 + \eta_{4n})}{\left((r_{1n}^H)^2 - (r_{2n}^H)^2\right)\left((\bar{\Omega}^H)^2 - (r_{2n}^H)^2\right)}, & B_{3n}^H &= \frac{\mathfrak{D}_n^H (-\zeta_{4n}(\bar{\Omega}^H)^2 + \eta_{4n})}{\left((r_{1n}^H)^2 - (\bar{\Omega}^H)^2\right)\left((r_{2n}^H)^2 - (\bar{\Omega}^H)^2\right)}, \\
 C_{1n}^H &= \frac{\mathcal{E}_n^H (-\zeta_{2n}(r_{1n}^H)^2 + \eta_{2n})}{\left((r_{2n}^H)^2 - (r_{1n}^H)^2\right)\left((g_n^H)^2 - (r_{1n}^H)^2\right)}, & C_{2n}^H &= \frac{\mathcal{E}_n^H (-\zeta_{2n}(r_{2n}^H)^2 + \eta_{2n})}{\left((r_{1n}^H)^2 - (r_{2n}^H)^2\right)\left((g_n^H)^2 - (r_{2n}^H)^2\right)}, \\
 C_{3n}^H &= \frac{\mathcal{E}_n^H (-\zeta_{2n}(g_n^H)^2 + \eta_{2n})}{\left((r_{1n}^H)^2 - (g_n^H)^2\right)\left((r_{2n}^H)^2 - (g_n^H)^2\right)}, & D_{1n}^H &= \frac{\mathcal{F}_n^H (-\zeta_{2n}(r_{1n}^H)^2 + \eta_{2n})}{\left((r_{2n}^H)^2 - (r_{1n}^H)^2\right)\left((\bar{\Omega}^H)^2 - (r_{1n}^H)^2\right)}, \\
 D_{2n}^H &= \frac{\mathcal{F}_n^H (-\zeta_{2n}(r_{2n}^H)^2 + \eta_{2n})}{\left((r_{1n}^H)^2 - (r_{2n}^H)^2\right)\left((\bar{\Omega}^H)^2 - (r_{2n}^H)^2\right)}, & D_{3n}^H &= \frac{\mathcal{F}_n^H (-\zeta_{2n}(\bar{\Omega}^H)^2 + \eta_{2n})}{\left((r_{1n}^H)^2 - (\bar{\Omega}^H)^2\right)\left((r_{2n}^H)^2 - (\bar{\Omega}^H)^2\right)}, \\
 C_n^H &= \frac{\beta_n^H g_n^H}{(\zeta_{1n}\zeta_{4n} - \zeta_{2n}\zeta_{3n})}, & \mathfrak{D}_n^H &= \frac{\mathcal{A}_n^H \bar{\Omega}^H}{(\zeta_{1n}\zeta_{4n} - \zeta_{2n}\zeta_{3n})}, & \mathcal{E}_n^H &= \frac{\beta_n^H g_n^H}{(\zeta_{1n}\zeta_{3n} - \zeta_{2n}^2)}, & \mathcal{F}_n^H &= \frac{\mathcal{A}_n^H \bar{\Omega}^H}{(\zeta_{1n}\zeta_{3n} - \zeta_{2n}^2)}.
 \end{aligned} \tag{41}$$

4.3. A Numerically Developed Solution Based on the MNMA ( $\varkappa = 1$ )

In this part, the dynamic response of the NT is sought by applying the Galerkin method based on the modal analysis approach. For this purpose, by multiplying both sides of Equations (32) and (33), respectively, by  $\delta\bar{w}^H$  and  $\delta\bar{\psi}^H$  and then by adding the obtained relations and applying the integral part by part, the following relation is obtained:

$$\begin{aligned}
 & \int_0^1 \left\{ \begin{aligned}
 & \delta\bar{w}^H \frac{\partial^2 \bar{w}^H}{\partial \tau^2} - \mu^2 \frac{\partial^2 (\delta\bar{w}^H)}{\partial \xi^2} \frac{\partial^2 \bar{w}^H}{\partial \tau^2} + \bar{k}_t^H \bar{w}^H d\bar{w}^H - \mathfrak{f}_1^2 \frac{\partial (\bar{w}^H)}{\partial \xi} \frac{\partial^2 \bar{\psi}^H}{\partial \tau^2} - \\
 & \mathfrak{f}_1^2 \mu^2 \frac{\partial^2 (\delta\bar{w}^H)}{\partial \xi^2} \frac{\partial^3 \bar{\psi}^H}{\partial \tau^2 \partial \xi} + \mathfrak{f}_2^2 \frac{\partial (\delta\bar{w}^H)}{\partial \xi} \frac{\partial^3 \bar{w}^H}{\partial \tau^2 \partial \xi} + \gamma_2^2 \mu^2 \frac{\partial^2 (\delta\bar{w}^H)}{\partial \xi^2} \frac{\partial^4 \bar{w}^H}{\partial \tau^2 \partial \xi^2} + \bar{k}_r^H \bar{\psi}^H \delta\bar{\psi}^H \\
 & - \mathfrak{f}_3^2 \delta\bar{w}^H \left( \frac{\partial \bar{\psi}^H}{\partial \xi} + \frac{\partial^2 \bar{w}^H}{\partial \xi^2} \right) + \frac{\partial (\delta\bar{w}^H)}{\partial \xi} \left( \gamma_4^2 \frac{\partial^2 \bar{\psi}^H}{\partial \xi^2} - \frac{\partial^3 \bar{\psi}^H}{\partial \xi^3} \right) + \delta\bar{\psi}_1^H \frac{\partial^2 \bar{\psi}^H}{\partial \tau^2} \\
 & + \mu^2 \frac{\partial (\delta\bar{\psi}^H)}{\partial \xi} \frac{\partial^3 \bar{\psi}^H}{\partial \tau^2 \partial \xi} - \gamma_6^2 \frac{\partial \bar{\psi}^H}{\partial \xi} \frac{\partial^2 \bar{w}^H}{\partial \tau^2} - \mu^2 \gamma_6^2 \frac{\partial \bar{\psi}^H}{\partial \xi} \frac{\partial^4 \bar{w}^H}{\partial \tau^2 \partial \xi^2} - \bar{k}_t^H \mu^2 \bar{w}^H \frac{\partial^2 (\delta\bar{w}^H)}{\partial \xi^2} + \\
 & \gamma_7^2 \delta\bar{\psi}^H \left( \bar{\psi}^H - \frac{\partial \bar{w}^H}{\partial \xi} \right) - \gamma_8^2 \frac{\partial (\delta\bar{\psi}^H)}{\partial \xi} \frac{\partial \bar{\psi}^H}{\partial \xi} + \gamma_9^2 \frac{\partial (\delta\bar{\psi}^H)}{\partial \xi} \frac{\partial^2 \bar{w}^H}{\partial \xi^2} - \mu^2 \bar{k}_r^H \bar{\psi}^H \frac{\partial^2 (\delta\bar{\psi}^H)}{\partial \xi^2} \end{aligned} \right\} d\xi \\
 & = \int_0^1 \left( \delta\bar{w}^H - \mu^2 \frac{\partial^2 (\delta\bar{w}^H)}{\partial \xi^2} \right) \left\{ \begin{aligned}
 & \bar{f}_m^H \left( 1 - \varkappa \frac{D^2 \bar{w}^H}{D\tau^2} \right) \delta(\xi - \xi_M) \mathbf{H}(\tau_f^H - \tau) + \\
 & \left( M_N \delta(\xi - \xi_M) \mathbf{H}(\tau_f^H - \tau) + 1 \right) \bar{f}_g^H \sin(\bar{\Omega}^H \tau) \end{aligned} \right\} d\xi.
 \end{aligned} \tag{42}$$

After substituting the discretized displacement fields  $\bar{w}^H(\xi, \tau) = \sum_{n=1}^{NM} \bar{a}_n^H(\tau) \phi_n^w(\xi)$  and  $\bar{\psi}^H(\xi, \tau) = \sum_{n=1}^{NM} \bar{b}_n^H(\tau) \phi_n^\psi(\xi)$  into Equation (42) and appropriately sorting the resulting relationships, the following system of ODEs is derived:

$$\begin{bmatrix} \left[ \bar{\mathbf{M}}_b^H \right]_{ij}^{ww} & \left[ \bar{\mathbf{M}}_b^H \right]_{ij}^{w\psi} \\ \left[ \bar{\mathbf{M}}_b^H \right]_{ij}^{\psi w} & \left[ \bar{\mathbf{M}}_b^H \right]_{ij}^{\psi\psi} \end{bmatrix} \begin{Bmatrix} \frac{d^2 \bar{a}_n^H}{d\tau^2} \\ d^2 \bar{b}_n^H \\ d\tau^2 \end{Bmatrix} + \begin{bmatrix} \left[ \bar{\mathbf{K}}_b^H \right]_{ij}^{ww} & \left[ \bar{\mathbf{K}}_b^H \right]_{ij}^{w\psi} \\ \left[ \bar{\mathbf{K}}_b^H \right]_{ij}^{\psi w} & \left[ \bar{\mathbf{K}}_b^H \right]_{ij}^{\psi\psi} \end{bmatrix} \begin{Bmatrix} \bar{a}_n^H \\ \bar{b}_n^H \end{Bmatrix} = \begin{Bmatrix} \left\{ \bar{\mathbf{f}}_b^H \right\}_i^w \\ \mathbf{0} \end{Bmatrix}, \tag{43}$$

in which the rows of these matrices are provided in the following form:

$$\begin{aligned} [\overline{\mathbf{M}}_b^H]_{ij}^{ww} &= 0.5(Y_{ij} + \Gamma_{ij}\mu^2 + \Gamma_{ij}\gamma_2^2 + \gamma_2^2(\mu\Gamma_{ij})^2) + \\ &M_N(1 + (i\pi\mu)^2)\sin(i\pi\xi_M)\sin(j\pi\xi_M)H(\tau_f^H - \tau), \end{aligned} \tag{44}$$

$$[\overline{\mathbf{M}}_b^H]_{ij}^{w\psi} = -0.5\gamma_1^2(\Xi_{ij} + \Pi_{ij}\mu^2), \tag{45}$$

$$[\overline{\mathbf{M}}_b^H]_{ij}^{\psi w} = -0.5\gamma_6^2(\Xi_{ij} + \Pi_{ij}\mu^2), \tag{46}$$

$$[\overline{\mathbf{M}}_b^H]_{ij}^{\psi\psi} = 0.5(Y_{ij} + \Gamma_{ij}\mu^2), \tag{47}$$

$$[\overline{\mathbf{C}}_b^H]_{ij}^{ww} = 2\beta^H M_N j \pi (1 + (i\pi\mu)^2)\sin(i\pi\xi_M)\cos(j\pi\xi_M)H(\tau_f^H - \tau), \tag{48}$$

$$\begin{aligned} [\overline{\mathbf{K}}_b^H]_{ij}^{ww} &= 0.5(\gamma_3^2\Gamma_{ij} + \Gamma_{ij}^2) + 0.5\bar{k}_t^H Y_{ij}(1 + (i\pi\mu)^2) - \\ &M_N(j\pi\beta^H)^2(1 + (i\pi\mu)^2)\sin(i\pi\xi_M)\sin(j\pi\xi_M)H(\tau_f^H - \tau), \end{aligned} \tag{49}$$

$$[\overline{\mathbf{K}}_b^H]_{ij}^{w\psi} = 0.5(\gamma_3^2\Xi_{ij} - \gamma_4^2\Pi_{ij}), \tag{50}$$

$$[\overline{\mathbf{K}}_b^H]_{ij}^{\psi w} = 0.5(\gamma_7^2\Xi_{ij} - \gamma_9^2\Pi_{ij}), \tag{51}$$

$$[\overline{\mathbf{K}}_b^H]_{ij}^{\psi\psi} = 0.5(\gamma_7^2 Y_{ij} + \gamma_8^2 \Gamma_{ij}) + 0.5\bar{k}_r^H Y_{ij}(1 + (i\pi\mu)^2), \tag{52}$$

$$\begin{aligned} \{\bar{\mathbf{f}}_b^H\}_i^w &= M_N(\gamma^H)^2(1 + (i\pi\mu)^2)\sin(i\pi\xi_m)H(\tau_f^H - \tau) + \\ &\left(M_N\sin(i\pi\xi_m)H(\tau_f^H - \tau) + \frac{(1 - \cos(i\pi))}{i\pi}\right)\bar{f}_g^H\sin(\overline{\Omega}^H\tau), \end{aligned} \tag{53}$$

where

$$\begin{aligned} Y_{ij} &= \delta_{ij}, \quad \Gamma_{ij} = ij\pi^2\delta_{ij}, \quad \Pi_{ij} = j^2\pi^3\delta_{ij}, \quad \Xi_{ij} = i\pi\delta_{ij}, \\ C_l^H &= \frac{\alpha_1}{l_b}\sqrt{\frac{J_6}{I_0}}, \quad \gamma^H = \frac{\sqrt{g l_b}}{C_l^H}, \quad M_N = \frac{M}{\rho_b A_b l_b}. \end{aligned} \tag{54}$$

Since the dynamical matrices based on the MNMA are time-dependent, we adopt the generalized Newmark- $\beta$  methodology [107] for the time discretization of the set of ODEs given in Equation (43) and then evaluate the elastodynamic fields of the nanobeam under the simultaneous influence of the MNO and medium excitations.

#### 4.4. Results and Discussion

A comprehensive parametric study on the vibrations of an NT in the presence of the effect of MNO and the stimulation of the elastic medium based on the theory of Rayleigh beams and higher-order shear is presented. Since the inertial effect of the MNO is also of great importance, both the results of the MNFA and MNMA are also demonstrated. To this end, carbon nanotubes with  $t_b = 0.34$  nm,  $r_m = 1$  nm,  $\rho_b = 2.3$  gr/cm<sup>3</sup>,  $E_b = 1$  TPa,  $\lambda = 20$ , and  $v_b = 0.2$  are considered. Also, in all the demonstrated figures, we consider  $e_0 a = 1$  nm,  $\beta = 0.6$ ,  $a_g = 10^{-15} l_b$ ,  $M_N = 0.3 \bar{k}_r^R = 10$ , and  $\bar{k}_t^R = 10$ , unless other values are clearly specified for them. In the presented graphs and tables, normalized speed, normalized displacement, and other parameter values are considered as:

$$\begin{aligned}
W_N &= \frac{\bar{w}(\xi, \tau)}{\bar{w}_{st}}, \quad \bar{w}_{st} = \frac{MgI_b^2}{48E_bI_b^*} = \frac{0.3\rho_b A_b^* g (I_b^*)^3}{48E_b I_b^*}, \quad \beta = \frac{\bar{\Omega}}{\omega_1}, \quad A_b^* = \pi \left( (r_o^*)^2 - (r_i^*)^2 \right), \\
A_b^* &= \pi \left( (r_o^*)^2 - (r_i^*)^2 \right), \quad I_b^* = \frac{\pi}{4} \left( (r_o^*)^4 - (r_i^*)^4 \right), \quad r_o^* = r_m^* + \frac{t_b}{2}, \quad r_i^* = r_m^* - \frac{t_b}{2}, \\
r_m^* &= 1 \text{ nm}, \quad V_N = \frac{v}{v^*}, \quad v^* = \frac{\pi}{I_b^*} \sqrt{\frac{E_b I_b^*}{\rho_b A_b^* \left( 1 + \frac{I_b^* \pi^2}{A_b^* (I_b^*)^2} \right) (1 + (\pi\mu)^2)}}.
\end{aligned} \tag{55}$$

In the next subsections, the correctness of the performed calculations is checked first, and then the influence of the parameters of the frequency and amplitude of the medium, the MNO's velocity and mass, and the stiffness of the torsional and translational spring on the deflection of the beam-like nanostructure are discussed.

#### 4.5. Validation Studies of the Suggested Models

##### 4.5.1. A Comparison between the MNFA's Results and Those of the MNMA

In order to ensure the accuracy and effectiveness of our calculations and models, we need to compare the results obtained from both analytical and numerical solutions for a specific scenario. This will help us confirm the correctness of our work and make any necessary adjustments if needed. To this end, we should lessen the transverse inertia of the nano-object, where herein such an issue is met by considering a negligible mass of the nano-object, i.e.,  $M_N = 0.01$ . In Table 1, the estimated normalized maximum deflection ( $W_{N,max}$ ) of the vibrated nanostructure by the surrounding medium and the MNO based on the MNFA and MNMA have been given for three levels of the amplitude of the vibrating medium (i.e.,  $a_g/l_b = 10^{-14}$ ,  $2 \times 10^{-14}$ , and  $3 \times 10^{-14}$ ), and the other properties of the MNO and surrounding medium are provided in the caption. As can be seen from Table 1, the percentage of the relative discrepancy between the results of the analytical and numerical methodologies is almost insignificant. Since these two approaches have been established completely distinctly, this result indicates that both models are capable of rationally predicting the dynamic response of the elastically embedded nanostructure in the presence of both medium excitation and MNO.

**Table 1.** Comparison between the results of the maximum normalized mid-span displacements based on the MNFA and MNMA for different slenderness ratios and excitation amplitudes of the elastic medium ( $e_0 a = 1$  nm,  $V_N = 0.6$ ,  $M_N = 0.01$ ,  $\beta = 0.3$ , and  $\bar{k}_r^R = 10$ ,  $\bar{k}_t^R = 10$ ).

$\lambda$		$W_{N,max}$					
		MNFA			MNMA		
		1	2	3	1	2	3
20	NRABT	1.846	3.671	5.497	1.896 (%2.86)	3.685 (%0.38)	5.517 (%0.36)
	NREBT	1.857	3.692	5.527	1.902 (%2.42)	3.762 (%1.2)	5.632 (%1.9)
50	NRABT	2.285	4.213	6.145	2.353 (%2.98)	4.238 (%0.59)	6.170 (%0.60)
	NREBT	2.297	4.219	6.150	2.345 (%2.09)	4.296 (%1.83)	6.266 (%1.87)
100	NRABT	5.169	6.998	8.859	5.212 (%0.83)	7.024 (%0.8)	8.953 (%1.06)
	NREBT	5.190	7.020	8.880	5.249 (%1.14)	7.104 (%1.2)	9.002 (%1.37)

#### 4.5.2. A Comparison between the Results Predicted by the Model and Those of Another Work in the Case of $a_g = 0$

In another comparison study, the results obtained from the proposed model with the results of Simsek [108] and Kiani [103], who, respectively, investigated the transverse vibrations of an NT acted upon by an MNO without considering its transverse inertia and the transverse vibrations of an NT under the action of harmonic environmental excitation. To properly compare the results of Simsek [108] with the proposed models based on the MNFA, the excitation of the elastic medium is omitted. Figure 2a has been added to compare the predicted results of our proposed model based on the MNFA-NRABT with those obtained by Simsek [108]. This subfigure showcases the predicted results of  $W_{N,max}$  in relation to  $l_b/d$  for three nonlocal factor levels ( $e_0a = 0, 1,$  and  $2$  nm) for  $a_g=0$  (the stationary elastic medium). Through this comparison, it is evident that our model's predicted results align well with those of Simsek [108] for each  $l_b/d$  value and all of the nonlocality levels considered. This indicates the dependability of our suggested model in accurately capturing the maximum deflection of the nanotube for a broad range of factors.

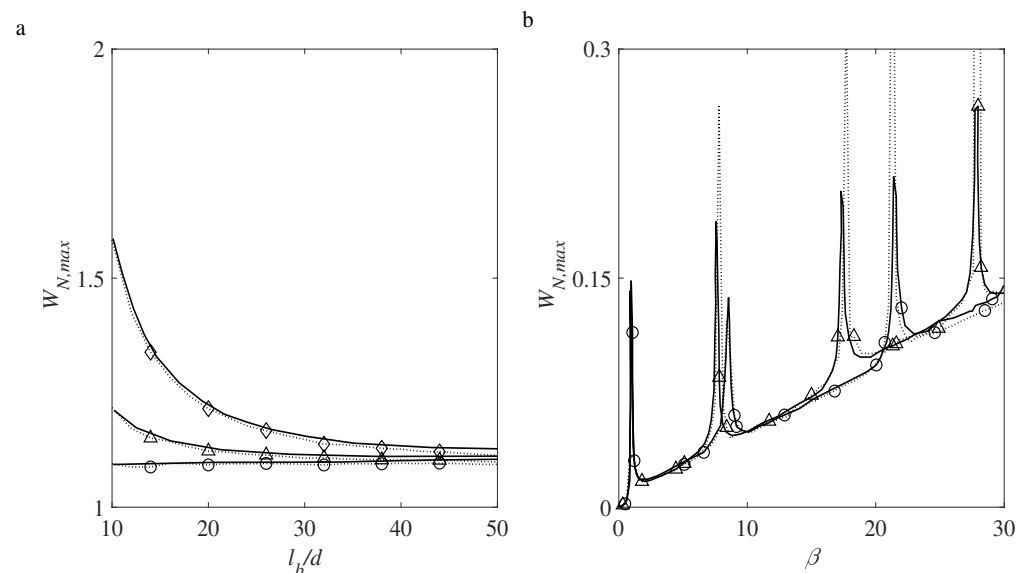


**Figure 2.** (a) Plots of  $W_{N,max}-l_b/d$  ( $r_m = 0.325$  nm,  $\rho_b = 2300$  kg/m<sup>3</sup>,  $t_b = 0.35$  nm,  $V_N = 0.1$ ,  $a_g = 0$ ); (○)  $e_0a = 0$ , (△)  $e_0a = 1$  nm, (◇)  $e_0a = 2$  nm; (—) Simsek [108], and (...) present study). (b) Plots of  $W_{N,max}-a_g$  ( $r_m = 3$  nm,  $\rho_b = 2500$  kg/m<sup>3</sup>,  $M_N = 0$ ,  $a_g = 0.01t_b$ ,  $\lambda = 30$ ); (—) Kiani [103], (...) present study; (○) NRABT, and (△) NREBT)retained.

#### 4.5.3. A Comparison between the Results Predicted by the Model and Those of Another Work in the Absence of the MNO

Also, to make a comparison between the results predicted by the model and those of Kiani [103], the MNO has been removed. The resulted obtained from this comparison investigation have been presented in Figure 2b. The plotted results in these subfigures reveal that reasonably good agreement between the results predicted by the proposed models and those of Kiani [103] can be achieved, indicating the rationality and high accuracy of the established models in this paper. It should be noticed that the present model possesses such generality that it could appropriately take into account both the transverse inertia effect of the MNO and the transverse excitation of the surrounding elastic medium, whose physical/structural mechanics interpretations have been not revealed yet.

Furthermore, our research focuses on exploring the effects of different factors on the  $W_{N,max}$  of beam-like nanostructures. These factors comprise medium excitation and MNOs, which play a crucial role in shaping the system's mechanical behavior. Herein, our chief objective is to comprehend the fundamental mechanisms involved and identify the crucial variables that impact these structures' performance. By thoroughly analyzing these

factors, we aim to devise better methods for managing and regulating these structures. This information will have far-reaching consequences for a diverse range of applications.

#### 4.6. Time History Analysis of the Mid-Span Deflection

The time-history plots of the NT's mid-span deflection based on the NREBT for three MNO's velocities (i.e.,  $V_N = 0.03, 0.3,$  and  $0.6$ ) and three amplitudes (i.e.,  $a_g/l_b = 0, 10^{-15},$  and  $2 \times 10^{-15}$ ) are illustrated in Figure 3a–c. The other properties of the MNO and medium excitation, as well as the mechanical interaction characteristics of the NT with the surrounding medium, are given in the caption. In the demonstrated subfigures, the dotted and solid lines are associated with the MNFA and the MNMA, respectively. For a fairly low MNO velocity (i.e.,  $V_N = 0.03$ ), the predicted results based on the MNMA are almost close to those obtained by employing MNFA, particularly in the absence of the excitation of the medium. Such a fact is chiefly related to the negligible amount of the transverse inertia effect of the MNO. In the case of  $a_g = 0$  and  $V_N = 0.03$ , we observe a symmetric time-history plot of  $W_{N,mid}-\tau/\tau_f$  w.r.t., the midspan point of the NT; however, by growing the amplitude of the medium excitation, the plotting results become unsymmetric, and this fact becomes highlighted as the MNO's velocity grows. In the presence of the medium excitation (see Figure 3b,c), the aforementioned symmetry is wholly violated even for a very small velocity of the MNO. The illustrated results reveal that the discrepancies between the MNFA-based and MNMA-based graphs increase with the growth of the MNO's velocity and medium excitation amplitude, representing the highlight of the MNO's transverse inertia. This pivotal issue guides us that for arriving at the near-to-exact mechanical response of the vibrating embedded NT subjected to the MNO, the influence of the MNO's inertia should be appropriately taken into account in the cases of MNOs with high velocities as well as vibrating mediums with high amplitudes.

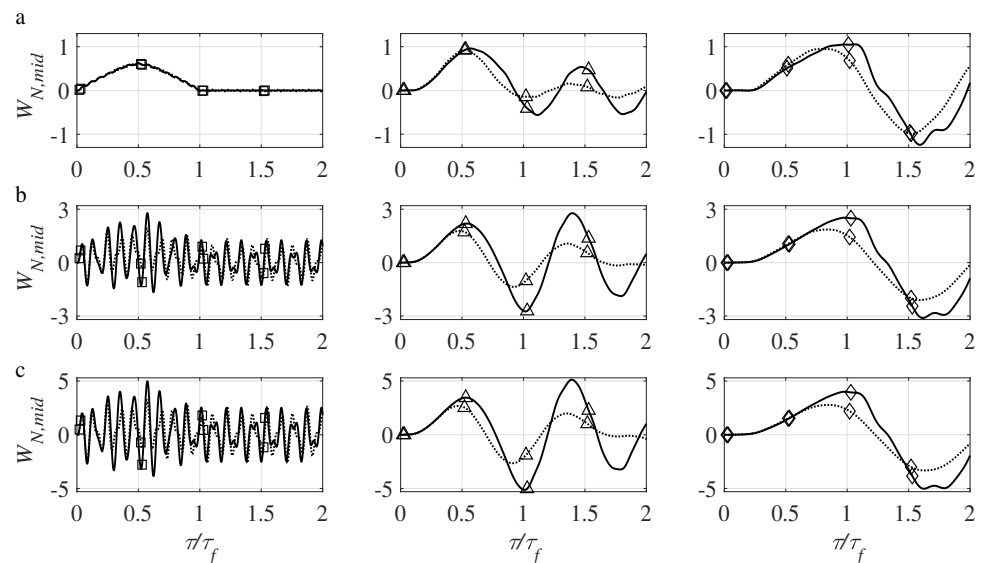


**Figure 3.** Plots of  $W_{N,mid}-\tau/\tau_f$  based on the NREBT: (a)  $a_g = 0$ , (b)  $a_g = 10^{-15}l_b$ , and (c)  $a_g = 2 \times 10^{-15}l_b$  ( $\beta = 0.6, M_N = 0.3, \bar{k}_r^R = \bar{k}_t^R = 10, \lambda = 20$ ; (...) MNFA, (—) MNMA; (□)  $V_N = 0.03$ , and (△)  $V_N = 0.3$ , and (◇)  $V_N = 0.6$ ).

The three-dimensional plots of the normalized mid-span deflection (i.e.,  $W_{N,mid} = \frac{\bar{w}(0.5,\tau)}{\bar{w}_{st}}$ ) as a function of the normalized MNO's velocity have been provided in Figure 4a,b for two cases  $a_g = 0$  and  $a_g = 10^{-15}l_b$ , respectively. In the absence of the medium excitation (i.e.,  $a_g = 0$ ; see Figure 4a), the illustrated results indicate that  $W_{N,mid}$  presents almost a symmetric curve w.r.t., the mid-span point at the small levels of the MNO's velocity. As the velocity of the MNO increases slightly, the symmetry of the time history plot of the mid-span deflection is violated such that the plot exhibits a moderately

positive value at the departure time of the MNO (i.e.,  $\tau/\tau_f = 1$ ). For higher levels of the MNO's velocity (i.e.,  $V_N > 0.7$ ), we observe an almost ascending trend, indicating that the maximum value of the deflection plot shifts from the course of vibration (i.e.,  $0 < \tau/\tau_f < 1$ ) to the course of excitation (i.e.,  $\tau/\tau_f > 1$ ). In the presence of a slight medium excitation of the amplitude  $a_g = 10^{-15}l_b$  (see Figure 4b), no specific symmetry of the deflection time-history plot is detectable for each level of the velocity. As is seen, for low levels of the MNO's velocity, the plots of  $W_{N,mid}-\tau/\tau_f$  demonstrate some fluctuations such that their amplitudes for specific levels of the MNO's velocity increase as time goes by during the course of excitation. In addition, for higher levels of the MNO's velocity (i.e.,  $V_N > 0.5$ ), we observe an almost ascending time-history plot of the mid-span deflection during the course of excitation, revealing the transfer of the peak point from that course to the free vibration course where their corresponding plots have been not given for the sake of brevity.

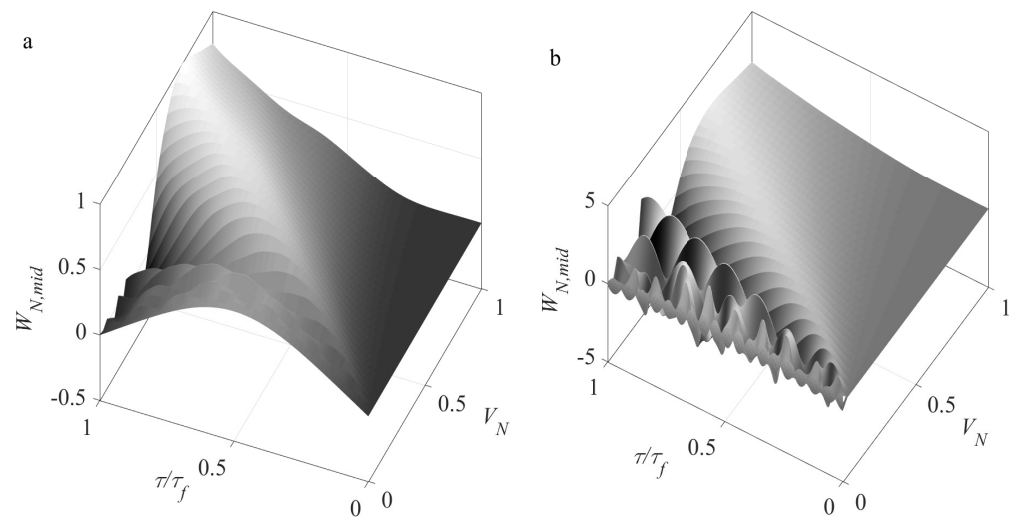


**Figure 4.** Three-dimensional plots of  $W_{N,mid}-V_N-\tau/\tau_f$  based on the NRABT: (a) in the absence of medium excitation ( $a_g = 0$ ); (b) in the presence of medium excitation ( $a_g = 10^{-15}l_b$ ); ( $\beta = 0.6$ ,  $M_N = 0.3$ ,  $\bar{k}_r^R = \bar{k}_t^R = 10$ , and  $\lambda = 20$ ).

#### 4.7. Influence of the Medium Excitation Parameters on the Maximum Deflection

In this subsection, the combined role of the medium and MNO's excitation parameters on the dynamic response of the nanobeam for the dimensionless velocities of 0.3, 0.6, and 0.9 for the MNO is examined. Figure 5 illustrates the impact of the medium excitation amplitude on  $W_{N,max}$ . By increasing the amplitude of the medium excitation, the predicted results by both established models increase almost linearly. In addition, it is expected that with the growth of the speed of the MNO, the maximum values of deflections generally increase, but due to the interaction between the medium and the moving load, a decrease in the dynamic response is detectable. As can be seen, the evaluated deflections based on the MNMA are usually greater than those obtained from the MNFA. Also, with the increase in the amplitude of medium excitation, the difference between the two mass and moving force approaches increases, which is the main reason for considering the transverse inertia in the MNMA.

According to Figure 5a,c, there are relative differences between the results of the NREBT and those of the NRABT in both the MNFA and MNMA for  $V_N = 0.3, 0.6$ , and  $0.9$  in the case of no medium excitation (i.e.,  $a_g = 0$ ) in order reach 20(62), 22(55), and 23(47), respectively intended meaning has been retained. . By increasing the amplitude of excitation, the relative discrepancies between the two nonlocally developed beam models based on the drawing results, for both moving force and mass approaches (except Figure 5a in the moving force approach), would generally decrease. Based on Figure 5a–c, for the moving

nanomass (moving nano-force) approach, such discrepancies touch 2(9), 2(2), and 24(5) percent, respectively.

In Figure 6, the influence of the medium excitation frequency on the maximum transverse displacements of the elastically rested nanostructure for different nano-object speeds is investigated. In this figure, we see several sudden ascending and descending branches in the maximum amount of displacements, which represent the existence of resonance states. Between these resonance points, the maximum transversal displacement of the nanostructure exhibits a sharp decrease, a mild increase, and finally a drastic increase as a function of the frequency of the excited medium.

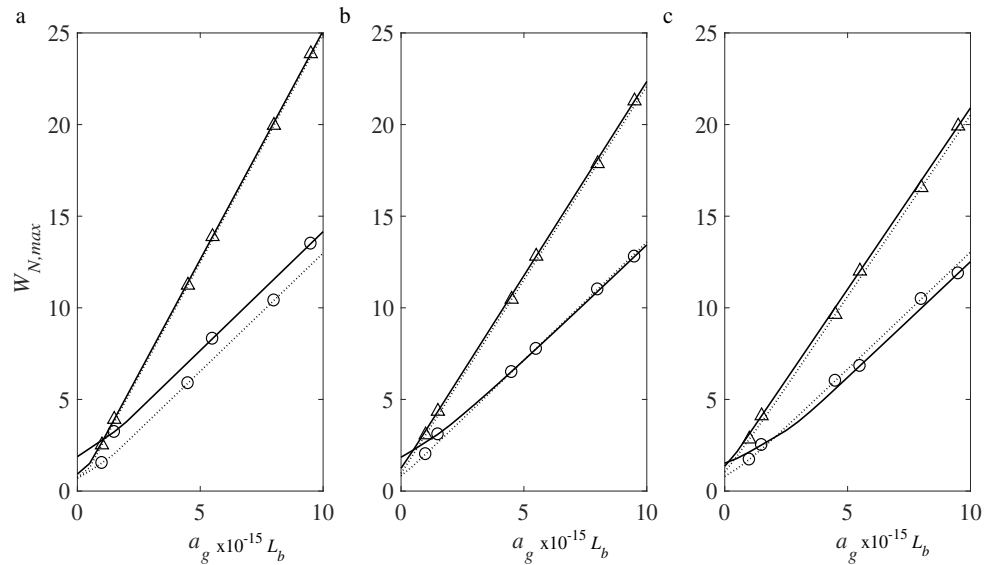


**Figure 5.** Plots of  $W_{N,max}-a_g$  for various MNO's speeds: (a)  $V_N = 0.3$ , (b)  $V_N = 0.6$ , and (c)  $V_N = 0.9$ ; (( $\circ$ ) MNFA, ( $\Delta$ ) MNMA; (...) NRABT, and (—) NREBT;  $\beta = 0.6$ ,  $a_g/l_b = 10^{-15}$ ,  $M_N = 0.3$ ,  $\bar{k}_t^R = 10$ , and  $\bar{k}_r^R = 10$ ).

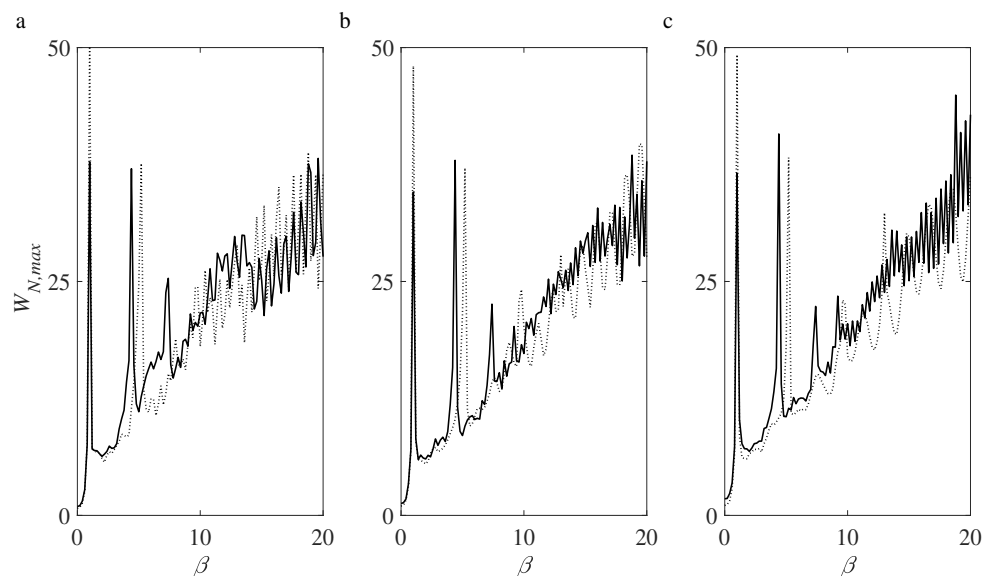


**Figure 6.** Plots of  $W_{N,max}-\beta$  based on the MNMA for various MNO's speeds: (a)  $V_N = 0.3$ , (b)  $V_N = 0.6$ , and (c)  $V_N = 0.9$ ; (...) NRABT, (—) NREBT;  $a_g/l_b = 10^{-15}$ ,  $M_N = 0.3$ ,  $\bar{k}_t^R = 10$ ,  $\bar{k}_r^R = 10$ ; and  $\beta = \frac{\bar{\omega}}{\omega_1}$ ).

#### 4.8. Influence of the MNO's Parameters on the Maximum Deflection

Figures 7 and 8 are drawn in order to more closely examine the effect of MNO's mass and velocity on the maximum dynamic response of the nanostructure embedded in the vibrating medium. In Figure 7, the dependency of the transverse displacement to the MNO's mass is methodically investigated for the normalized speeds of 0.3, 0.6, and 0.9. It can be clearly seen that with the growth of the nano-object mass, displacements grow. Since the transverse inertia effect of the MNO is taken into account in the MNMA, with the increase in the mass of the nano-object, the inertial effect increases, and thus the difference between the two considered approaches of moving nanomass and nanoforce (i.e., MNFA and MNMA) increases. For example, in the case of  $M_N = 0.4$ , the NRABT(NREBT) predicts that the relative differences between the predicted maximum deflections based on the MNFA and those of the MNMA for  $V_N = 0.3, 0.6$ , and  $0.9$  take 42.5(39.7)%, 39.8(41.5)%, and 45.5(53.5)%, respectively. This issue also reveals that the nonlocal shear deformable model exhibits a more inertial effect of the MNO compared to the nonlocal Rayleigh beam-based model, particularly at high levels of the MNO's speed.

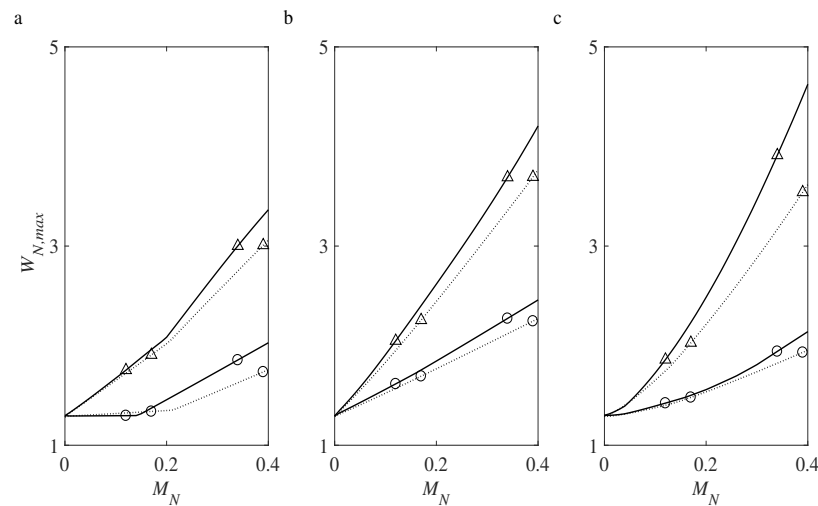


**Figure 7.** Plots of  $W_{N,max}$ -MNO's mass for various MNO's speeds: (a)  $V_N = 0.3$ , (b)  $V_N = 0.6$ , and (c)  $V_N = 0.9$ ; (( $\circ$ ) MNFA, ( $\triangle$ ) MNMA; (...) NRABT, and (—) NREBT;  $\beta = 0.6$ ,  $a_g/l_b = 10^{-15}$ , and  $\bar{k}_t^R = 10$ ,  $\bar{k}_r^R = 10$ ).

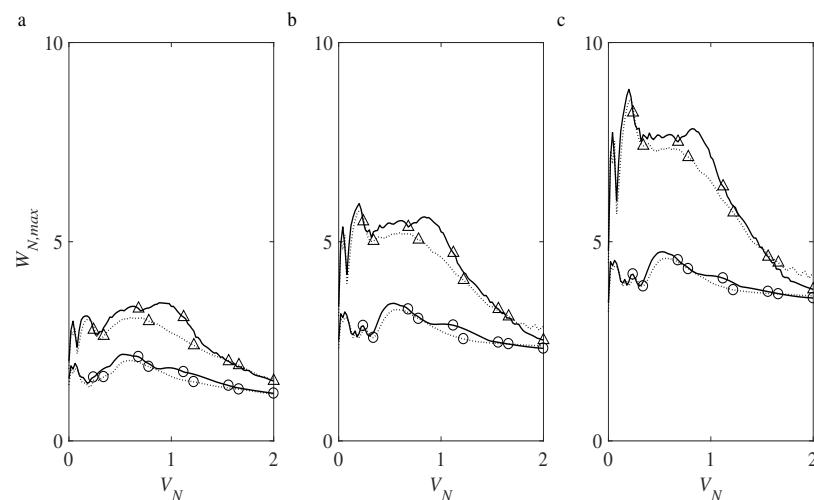


**Figure 8.** Plots of  $W_{N,max}$ -MNO's speed for three levels of the excitation amplitude of the elastic medium: (a)  $a_g = 10^{-15} l_b$ , (b)  $a_g = 2 \times 10^{-15} l_b$ , and (c)  $a_g = 3 \times 10^{-15} l_b$ ; (( $\circ$ ) MNFA, ( $\triangle$ ) MNMA; (...) NRABT, and (—) NREBT;  $M_N = 0.3$ , and  $\bar{k}_t^R = \bar{k}_r^R = 10$ ).

According to the plotted results in Figure 7, the relative discrepancy between the two newly established models (i.e., shear effect) is initially negligible, but with the growth of the MNO's mass, such a difference generally grows. In other words, the shear effect commonly increases with the mass of the MNO, irrespective of considering its inertia effect. For instance, for the case of  $M_N = 0.4$ , these relative differences based on the MNMA(MNFA) for the MNO's speeds of  $V_N = 0.3, 0.6,$  and  $0.9$  reach 7(13.3)%, 10(7.6)%, and 21(8.5)% percent, respectively.

Figure 8 demonstrates  $W_{N,max}$  in terms of the MNO's speed for various amplitudes of the medium excitation. As the dimensionless MNO's speed increases up to 1,  $W_{N,max}$  generally fluctuate such that these fluctuations are more obvious in the range of  $V_N \in [0, 0.4]$ , and then the plot follows a descending trend. In such a velocity interval (i.e.,  $V_N > 1$ ), the values of  $W_{N,max}$  are commonly lower than those obtained from the loading of the purely excited medium (i.e.,  $v = 0$ ). As is seen, the maximum possible magnitudes of  $W_{N,max}$  based on the MNMA for the cases of  $a_g / (10^{-15}l_b) = 1, 2,$  and  $3$  are, respectively, obtained as 3.45, 5.96, and 8.82, taking place at  $V_N = 0.95, 0.2,$  and  $0.2$ . Additionally,  $W_{N,max}$  generally grows with the increase in the amplitude of medium excitation, where the more detailed trend of  $W_{N,max}$  as a function of the amplitude was displayed in Section 4.7.

Upon a closer examination of the presented findings, it becomes apparent that the discrepancy between the two models (i.e., shear effect) varies in an oscillatory pattern based on the speed of the MNO; for example, the maximum values of this difference on the basis of the MNMA(MNFA) in the cases of  $a_g / (10^{-15}l_b) = 1, 2,$  and  $3$  would be about 20.5%(13%), 14.3%(9.5%), and 12.2%(6.2%), respectively, for the understudied range of the MNO's speed (i.e.,  $0 < V_N < 2$ ). Most of these discrepancies also occur close to  $V_N = 1$ ; for instance, the results obtained based on the MNMA show that the maximum discrepancies between the NRABT and NREBT deflections for the above-mentioned three excitation amplitudes (i.e.,  $a_g / (10^{-15}l_b) = 1, 2,$  and  $3$ ) take place at around  $V_N = 1, 0.93,$  and  $0.9$ . As is seen, the shear effect would commonly reduce with increased amplitude of the medium excitation in the range of  $10^{-15}l_b < a_g < 3 \times 10^{-15}l_b$ .

The plotted results based on both the NREBT and NRABT reveal that the absolute maximum inertia effect for the cases of  $a_g / (10^{-15}l_b) = 1, 2,$  and  $3$  occurs at about  $V_N = 0.18, 0.18,$  and  $0.2$  such that the relative discrepancies between their results based on the NREBT-MNMA and those of the NREBT-MNFA reach 53.8%, 55.6%, and 54.9%, respectively. In addition, other relative maximum points of the plots of these discrepancies for the above-mentioned amplitudes of the medium excitation take place at  $V_N = 0.9, 0.9,$  and  $0.86$ , which are reported to be 47.8%, 47.2%, and 45.9%, respectively. For MNO's speeds greater than these values,  $W_{N,max}$  of the nanostructure embedded in the vibrating medium commonly follows a descending trend, indicating that the maximum deflection lessens with the increase in the MNO's speed.

#### 4.9. Influence of the Substrate Parameters on the Maximum Deflection

In Figures 9 and 10, respectively, the impacts of the stiffness of torsional and translational springs of the elastic bed on the  $W_{N,max}$  response of the elastically rested nanostructure under the combined excitations of the MNO and harmonic bed excitation are explored for different values of the MNO's velocity. In the moving force approach, with the increase in stiffness of the torsional and transmission springs,  $W_{N,max}$  lessens sharply at first; then, they do not substantially alter. In this approach, by increasing the speed of the nano-object to 0.9, the relative discrepancies between the predicted deflections by the NRABT and those of the NREBT increase, and the main reason for this fact is considering the effect of shear deformation in the NREBT's formulations. In the MNMA as its corresponding results demonstrated in Figure 9, the two established models exhibit different trends so that in the NRABT,  $W_{N,max}$  first experiences a downward trend; then, after a temporary upward trend, it starts to decrease again. However, according to the plotted results on the basis of the MNMA in Figure 9a, the two beam theories exhibit different trends. Concerning the results predicted by the NRABT, with the increase in torsional spring stiffness,  $W_{N,max}$

first demonstrates a downward trend; then, after a temporary upward trend, it starts to decrease again, while the NREBT-based graphs of  $W_{N,max}$  begin to oscillate after a sharp decrease.

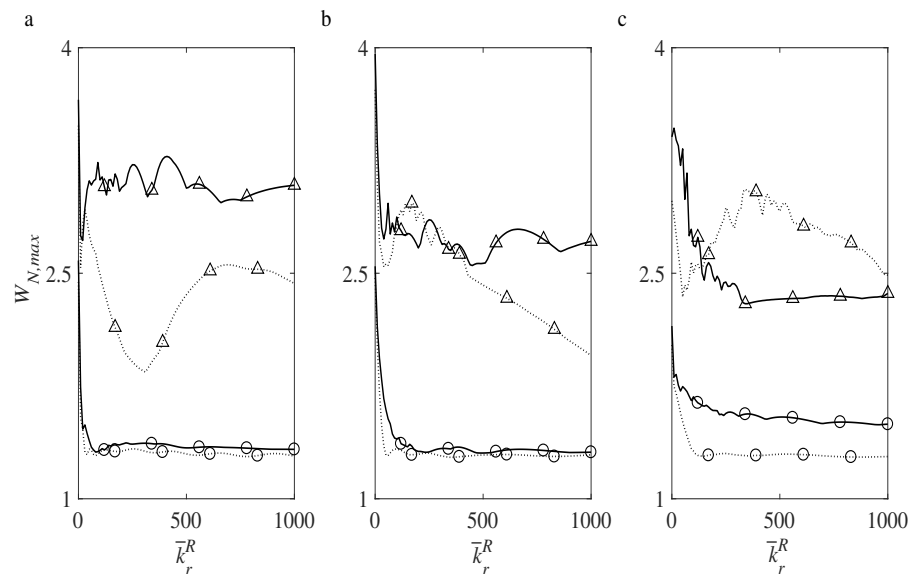


**Figure 9.** Graphs of  $W_{N,max}-\bar{k}_r^R$  for various MNO's speeds: (a)  $V_N = 0.3$ , (b)  $V_N = 0.6$ , and (c)  $V_N = 0.9$ ; (( $\circ$ ) MNFA, ( $\triangle$ ) MNMA; (...) NRABT, and (—) NREBT;  $\beta = 0.6$ ,  $a_g/l_b = 10^{-15}$ ,  $M_N = 0.3$ , and  $\bar{k}_t^R = 10$ ).

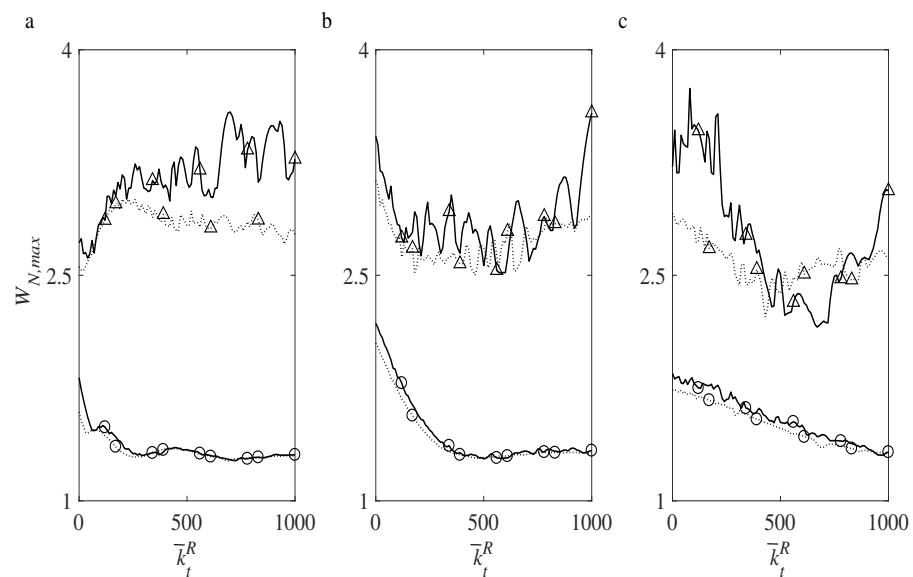


**Figure 10.** Graphs of  $W_{N,max}-\bar{k}_t^R$  for various MNO's speeds: (a)  $V_N = 0.3$ , (b)  $V_N = 0.6$ , and (c)  $V_N = 0.9$ ; (( $\circ$ ) MNFA, ( $\triangle$ ) MNMA; (...) NRABT, and (—) NREBT;  $\beta = 0.6$ ,  $a_g/l_b = 10^{-15}$ ,  $M_N = 0.3$ , and  $\bar{k}_r^R = 10$ ).

The changes in the dynamic response of the nanostructure are different depending on the stiffness of the translational spring for the MNMA (Figure 10). In Figure 10a, the maximum lateral displacement of both beam theories changes in an oscillating manner after an upward movement, whereas Figure 10b,c display that the predicted results lessen to reach their lowest value and then start to rise, while  $W_{N,max}$  based on the MNMA-NREBT commences to oscillate after a sharp decrease. According to the plotted results in Figures 9 and 10, the relative difference between the results of the two established models in both the MNFA and MNMA as a function of rotational and translational stiffness of the adjacent medium varies in an oscillating manner. According to Figure 9a–c for the vases of  $V_N = 0.3$ , 0.6, and 0.9, the maximum relative discrepancy between these two models in the MNMA

(MNFA) reaches 41(12), 27(18), and 33(21) percent, respectively, while these maximum relative discrepancies for the above-mentioned MNO's velocities based on Figure 10a–c would be equal to 21(12), 19(6), and 25(6) percent, respectively.

## 5. Concluding Remarks

Vibrations of embedded tube-like nanostructures translocating MNOs in the presence of a vibrating elastic medium are appropriately unlocked in the context of the nonlocal elasticity theory. To this end, the governing equations of the problem based on Rayleigh and Reddy–Bickford beam theories are methodically obtained. Using suitable vibration modes, both analytical and numerical solutions are developed to properly capture the nonlocal dynamic deflection of the nanostructure based on the MNFA (excluding the inertial effect) and MNMA (including the inertial effect). To show the precision of the developed models, their results are successfully checked with those of other researchers in particular cases. In continuing, the impacts of the chief characteristics of the MNO (mass and velocity), the main features of the medium excitation (amplitude and frequency), and the properties of the surrounding medium (lateral and rotational stiffness) on the maximum deflection are examined in detail.

The results obtained indicate that by increasing the amplitude of medium excitation, the results of both nonlocally established models increase almost linearly. Due to the interactional effects of the medium and the moving load on the nonlocal vibrations, for  $a_g/l_b < 3 \times 10^{-15}$ , as the dimensionless MNO's speed increases up to 1, the maximum dynamic deflection generally exhibits a fluctuation trend such that most of these oscillations occur in  $V_N \in [0, 0.4]$ , and then it generally lessens with the growth of the MNO's speed. On the other hand, with the increase in the frequency of the medium excitation up to the fundamental frequency (approaching resonant state), the maximum dynamic deflection sharply grows. The maximum transversal displacements of the nanosystem between two resonance states generally exhibit a U-shape trend. In addition, with the increase in the mass of the nano-object, the effect of inertia increases, and thus the discrepancy between the results of the MNFA and MNMA increases. Because of the lateral inertial effect of the MNO, the maximum dynamic deflections of the nanotube carrying the nano-object based on the MNMA are higher than those predicted by the MNFA.

It is hoped that this research could provide a solid basis for further investigations into the vibrations of more complex tube-like nanosystems (for example, vertically aligned membranes and jungles of nanotubes) embedded in a vibrating medium for delivering MNOs. In addition, artificial intelligence (AI) and machine learning (ML) have become two of the most crucial and rapidly evolving technologies of the digital age, with a diverse range of applications in various branches of engineering sciences [109–115]. Computers now have the ability to execute tasks that were once thought to be the exclusive domain of human intelligence, including decision-making, pattern recognition, and problem-solving. These technologies are gradually expected to revolutionize the way we approach complex challenges in nanoscale modeling and mechanical behavior predictions.

**Author Contributions:** Simulation and figure preparation, X.M. and M.R.; extraction of the formulations/reasons: X.M. and M.R.; conceptualization: K.K.; writing and editing, X.M., K.K. and A.N.; supervision, K.K. and A.N.; and project administration, K.K. All authors have read and agreed to the published version of the manuscript.

**Funding:** This research received no external funding.

**Institutional Review Board Statement:** Not applicable.

**Informed Consent Statement:** Not applicable.

**Data Availability Statement:** Data are available upon request.

**Acknowledgments:** The financial support of the corresponding universities of the authors from the present work is highly appreciated.

**Conflicts of Interest:** The authors declare no conflict of interest.

## References

1. Coleman, J.N.; Khan, U.; Blau, W.J.; Gun'ko, Y.K. Small but strong: A review of the mechanical properties of carbon nanotube–polymer composites. *Carbon* **2006**, *44*, 1624–1652. [[CrossRef](#)]
2. Xie, S.; Li, W.; Pan, Z.; Chang, B.; Sun, L. Mechanical and physical properties on carbon nanotube. *J. Phys. Chem. Solids* **2000**, *61*, 1153–1158. [[CrossRef](#)]
3. Oh, E.S. Elastic properties of boron-nitride nanotubes through the continuum lattice approach. *Mater. Lett.* **2010**, *64*, 859–862. [[CrossRef](#)]
4. Santosh, M.; Maiti, P.K.; Sood, A.K. Elastic properties of boron nitride nanotubes and their comparison with carbon nanotubes. *J. Nanosci. Nanotechnol.* **2009**, *9*, 5425–5430. [[CrossRef](#)]
5. Whitby, M.; Quirke, N. Fluid flow in carbon nanotubes and nanopipes. *Nat. Nanotechnol.* **2007**, *2*, 87–94. [[CrossRef](#)]
6. Majumder, M.; Chopra, N.; Andrews, R.; Hinds, B.J. Enhanced flow in carbon nanotubes. *Nature* **2005**, *438*, 44. [[CrossRef](#)]
7. Thomas, J.A.; McGaughey, A.J. Reassessing fast water transport through carbon nanotubes. *Nano Lett.* **2008**, *8*, 2788–2793. [[CrossRef](#)]
8. Won, C.Y.; Aluru, N.R. Water permeation through a subnanometer boron nitride nanotube. *J. Am. Chem. Soc.* **2007**, *129*, 2748–2749. [[CrossRef](#)]
9. Zhang, Q.L.; Yang, R.Y. Fast transport of water molecules across carbon nanotubes induced by static electric fields. *Chem. Phys. Lett.* **2016**, *644*, 201–204. [[CrossRef](#)]
10. Ezzati Nazhad Dolatabadi, J.; Omid, Y.; Losic, D. Carbon nanotubes as an advanced drug and gene delivery nanosystem. *Curr. Nanosci.* **2011**, *7*, 297–314. [[CrossRef](#)]
11. Pastorin, G.; Wu, W.; Wieckowski, S.; Briand, J.P.; Kostarelos, K.; Prato, M.; Bianco, A. Double functionalisation of carbon nanotubes for multimodal drug delivery. *Chem. Commun.* **2006**, *11*, 1182–1184. [[CrossRef](#)]
12. Sun, X.; Su, X.; Wu, J.; Hinds, B.J. Electrophoretic transport of biomolecules through carbon nanotube membranes. *Langmuir* **2011**, *27*, 3150–3156. [[CrossRef](#)] [[PubMed](#)]
13. Chen, Q.; Liang, L.; Zhang, Z.; Wang, Q. Release of an encapsulated peptide from carbon nanotubes driven by electric fields: A molecular dynamics study. *ACS Omega* **2021**, *6*, 27485–27490. [[CrossRef](#)] [[PubMed](#)]
14. Song, W.; Pang, P.; He, J.; Lindsay, S. Optical and electrical detection of single-molecule translocation through carbon nanotubes. *ACS Nano* **2013**, *7*, 689–694. [[CrossRef](#)]
15. Jue, M.L.; Buchsbaum, S.F.; Chen, C.; Park, S.J.; Meshot, E.R.; Wu, K.J.J.; Fornasiero, F. Ultra-Permeable Single-Walled Carbon Nanotube Membranes with Exceptional Performance at Scale. *Adv. Sci.* **2020**, *7*, 2001670. [[CrossRef](#)] [[PubMed](#)]
16. Joseph, S.; Aluru, N.R. Why are carbon nanotubes fast transporters of water? *Nano Lett.* **2008**, *8*, 452–458. [[CrossRef](#)]
17. Pantarotto, D.; Briand, J.P.; Prato, M.; Bianco, A. Translocation of bioactive peptides across cell membranes by carbon nanotubes. *Chem. Commun.* **2004**, *1*, 16–17. [[CrossRef](#)] [[PubMed](#)]
18. Bianco, A.; Kostarelos, K.; Prato, M. Applications of carbon nanotubes in drug delivery. *Curr. Opin. Chem. Biol.* **2005**, *9*, 674–679. [[CrossRef](#)]
19. Liu, X.; Marangon, I.; Melinte, G.; Wilhelm, C.; Ménard-Moyon, C.; Pichon, B.P.; Ersen, O.; Aubertin, K.; Baaziz, W.; Pham-Huu, C.; et al. Design of covalently functionalized carbon nanotubes filled with metal oxide nanoparticles for imaging, therapy, and magnetic manipulation. *ACS Nano* **2014**, *8*, 11290–11304. [[CrossRef](#)]
20. Gao, H.; Kong, Y.; Cui, D.; Ozkan, C.S. Spontaneous insertion of DNA oligonucleotides into carbon nanotubes. *Nano Lett.* **2003**, *3*, 471–473. [[CrossRef](#)]
21. Chen, M.; Zang, J.; Xiao, D.; Zhang, C.; Liu, F. Nanopumping molecules via a carbon nanotube. *Nano Res.* **2009**, *2*, 938–944. [[CrossRef](#)]
22. Arsawang, U.; Saengsawang, O.; Rungrotmongkol, T.; Sornmee, P.; Wittayanarakul, K.; Remsungnen, T.; Hannongbua, S. How do carbon nanotubes serve as carriers for gemcitabine transport in a drug delivery system? *J. Mol. Graph. Model.* **2011**, *29*, 591–596. [[CrossRef](#)]
23. Xue, Q.; Jing, N.; Chu, L.; Ling, C.; Zhang, H. Release of encapsulated molecules from carbon nanotubes using a displacing method: A MD simulation study. *RSC Adv.* **2012**, *2*, 6913–6920. [[CrossRef](#)]
24. Longhurst, M.J.; Quirke, N. Temperature-driven pumping of fluid through single-walled carbon nanotubes. *Nano Lett.* **2007**, *7*, 3324–3328. [[CrossRef](#)] [[PubMed](#)]
25. Insepov, Z.; Wolf, D.; Hassanein, A. Nanopumping using carbon nanotubes. *Nano Lett.* **2006**, *6*, 1893–1895. [[CrossRef](#)] [[PubMed](#)]
26. Xue, Q.; Xia, D.; Lv, C.; Jing, N.; Ling, C. Molecule delivery by the domino effect of carbon nanotubes. *J. Phys. Chem. C* **2011**, *115*, 20471–20480. [[CrossRef](#)]
27. Eringen, A.C.; Edelen, D. On nonlocal elasticity. *Int. J. Eng. Sci.* **1972**, *10*, 233–248. [[CrossRef](#)]
28. Eringen, A.C. Linear theory of nonlocal elasticity and dispersion of plane waves. *Int. J. Eng. Sci.* **1972**, *10*, 425–435. [[CrossRef](#)]
29. Eringen, A.C. Nonlocal elasticity and waves. In *Continuum Mechanics Aspects of Geodynamics and Rock Fracture Mechanics, Proceedings of the NATO Advanced Study Institute, Reykjavik, Iceland, 11–20 August 1974*; Springer: New York, NY, USA, 1974; pp. 81–105.
30. Eringen, A.C. Vistas of nonlocal continuum physics. *Int. J. Eng. Sci.* **1992**, *30*, 1551–1565. [[CrossRef](#)]

31. Eringen, A.C. Nonlocal Continuum Field Theories. *Appl. Mech. Rev.* **2002**, *56*, B20–B22.
32. Mindlin, R.D.; Eshel, N. On first strain-gradient theories in linear elasticity. *Int. J. Solids Struct.* **1968**, *4*, 109–124. [[CrossRef](#)]
33. Mindlin, R.D. Second gradient of strain and surface-tension in linear elasticity. *Int. J. Solids Struct.* **1965**, *1*, 417–438. [[CrossRef](#)]
34. Lim, C.W.; Zhang, G.; Reddy, J. A higher-order nonlocal elasticity and strain gradient theory and its applications in wave propagation. *J. Mech. Phys. Solids* **2015**, *78*, 298–313. [[CrossRef](#)]
35. Toupin, R.A. Theories of elasticity with couple-stress. *Arch. Ration. Mech. Anal.* **1964**, *17*, 85–112. [[CrossRef](#)]
36. Toupin, R. Elastic materials with couple-stresses. *Arch. Ration. Mech. Anal.* **1962**, *11*, 385–414. [[CrossRef](#)]
37. Gurtin, M.E.; Murdoch, I.A. A continuum theory of elastic material surfaces. *Arch. Ration. Mech. Anal.* **1975**, *57*, 291–323. [[CrossRef](#)]
38. Gurtin, M.E.; Murdoch, A.I. Effect of surface stress on wave propagation in solids. *J. Appl. Phys.* **1976**, *47*, 4414–4421. [[CrossRef](#)]
39. Duan, W.H.; Wang, C.M.; Zhang, Y.Y. Calibration of nonlocal scaling effect parameter for free vibration of carbon nanotubes by molecular dynamics. *J. Appl. Phys.* **2007**, *101*, 024305. [[CrossRef](#)]
40. Ansari, R.; Rouhi, H.; Sahmani, S. Calibration of the analytical nonlocal shell model for vibrations of double-walled carbon nanotubes with arbitrary boundary conditions using molecular dynamics. *Int. J. Mech. Sci.* **2011**, *53*, 786–792. [[CrossRef](#)]
41. Huang, L.Y.; Han, Q.; Liang, Y.J. Calibration of nonlocal scale effect parameter for bending single-layered graphene sheet under molecular dynamics. *Nano* **2012**, *7*, 1250033. [[CrossRef](#)]
42. Challamel, N.; Lerbet, J.; Wang, C.M.; Zhang, Z. Analytical length scale calibration of nonlocal continuum from a microstructured buckling model. *Z. Angew. Math. Mech.* **2014**, *94*, 402–413. [[CrossRef](#)]
43. Fernández-Sáez, J.; Zaera, R.; Loya, J.A.; Reddy, J. Bending of Euler–Bernoulli beams using Eringen’s integral formulation: A paradox resolved. *Int. J. Eng. Sci.* **2016**, *99*, 107–116. [[CrossRef](#)]
44. Challamel, N.; Reddy, J.N.; Wang, C.M. Eringen’s stress gradient model for bending of nonlocal beams. *J. Eng. Mech.* **2016**, *142*, 04016095. [[CrossRef](#)]
45. Shaat, M.; Faroughi, S.; Abasiniyan, L. Paradoxes of differential nonlocal cantilever beams: Reasons and a novel solution. *arXiv* **2017**, arXiv:1802.01494.
46. Ke, L.L.; Xiang, Y.; Yang, J.; Kitipornchai, S. Nonlinear free vibration of embedded double-walled carbon nanotubes based on nonlocal Timoshenko beam theory. *Comp. Mater. Sci.* **2009**, *47*, 409–417. [[CrossRef](#)]
47. Yang, J.; Ke, L.L.; Kitipornchai, S. Nonlinear free vibration of single-walled carbon nanotubes using nonlocal Timoshenko beam theory. *Physica E* **2010**, *42*, 1727–1735. [[CrossRef](#)]
48. Kiani, K. Magnetically affected single-walled carbon nanotubes as nanosensors. *Mech. Res. Commun.* **2014**, *60*, 33–39. [[CrossRef](#)]
49. Kiani, K. Free vibration of in-plane-aligned membranes of single-walled carbon nanotubes in the presence of in-plane-unidirectional magnetic fields. *J. Vib. Control* **2016**, *22*, 3736–3766. [[CrossRef](#)]
50. Kiani, K. Longitudinally varying magnetic field influenced transverse vibration of embedded double-walled carbon nanotubes. *Int. J. Mech. Sci.* **2014**, *87*, 179–199. [[CrossRef](#)]
51. Ansari, R.; Rouhi, H.; Sahmani, S. Free vibration analysis of single-and double-walled carbon nanotubes based on nonlocal elastic shell models. *J. Vib. Control* **2014**, *20*, 670–678. [[CrossRef](#)]
52. Li, C.; Li, S.; Yao, L.; Zhu, Z. Nonlocal theoretical approaches and atomistic simulations for longitudinal free vibration of nanorods/nanotubes and verification of different nonlocal models. *Appl. Math. Model.* **2015**, *39*, 4570–4585. [[CrossRef](#)]
53. Kiani, K. Characterization of free vibration of elastically supported double-walled carbon nanotubes subjected to a longitudinally varying magnetic field. *Acta Mech.* **2013**, *224*, 3139–3151. [[CrossRef](#)]
54. Rakrak, K.; Zidour, M.; Heireche, H.; Bousahla, A.A.; Chemi, A. Free vibration analysis of chiral double-walled carbon nanotube using nonlocal elasticity theory. *Adv. Nano Res.* **2016**, *4*, 031. [[CrossRef](#)]
55. Rahmanian, M.; Torkaman-Asadi, M.A.; Firouz-Abadi, R.D.; Kouchakzadeh, M.A. Free vibrations analysis of carbon nanotubes resting on Winkler foundations based on nonlocal models. *Physica B* **2016**, *484*, 83–94. [[CrossRef](#)]
56. Nikkhoo, A.; Zolfaghari, S.; Kiani, K. A simplified-nonlocal model for transverse vibration of nanotubes acted upon by a moving nanoparticle. *J. Braz. Soc. Mech. Sci.* **2017**, *39*, 4929–4941. [[CrossRef](#)]
57. Dihaj, A.; Zidour, M.; Meradjah, M.; Rakrak, K.; Heireche, H.; Chemi, A. Free vibration analysis of chiral double-walled carbon nanotube embedded in an elastic medium using nonlocal elasticity theory and Euler Bernoulli beam model. *Struct. Eng. Mech.* **2018**, *65*, 335–342.
58. Su, Y.C.; Cho, T.Y. Free vibration of a single-walled carbon nanotube based on the nonlocal Timoshenko beam model. *J. Mech.* **2021**, *37*, 616–635. [[CrossRef](#)]
59. Kiani, K. Nonlocal and shear effects on column buckling of single-layered membranes from stocky single-walled carbon nanotubes. *Compos. Part B-Eng.* **2015**, *79*, 535–552. [[CrossRef](#)]
60. Setoodeh, A.R.; Khosrownejad, M.; Malekzadeh, P. Exact nonlocal solution for postbuckling of single-walled carbon nanotubes. *Physica E* **2011**, *43*, 1730–1737. [[CrossRef](#)]
61. Shen, H.S.; Zhang, C.L. Torsional buckling and postbuckling of double-walled carbon nanotubes by nonlocal shear deformable shell model. *Compos. Struct.* **2010**, *92*, 1073–1084. [[CrossRef](#)]
62. Ansari, R.; Faghih Shojaei, M.; Mohammadi, V.; Gholami, R.; Rouhi, H. Buckling and postbuckling of single-walled carbon nanotubes based on a nonlocal Timoshenko beam model. *Z. Angew. Math. Mech.* **2015**, *95*, 939–951. [[CrossRef](#)]

63. Jamali, M.; Shojaee, T.; Mohammadi, B. Analytical buckling and post-buckling characteristics of Mindlin micro composite plate with central opening by use of nonlocal elasticity theory. *J. Comput. Appl. Mech.* **2020**, *51*, 231–238.
64. Malikan, M.; Uglov, N.S.; Eremeyev, V.A. On instabilities and post-buckling of piezomagnetic and flexomagnetic nanostructures. *Int. J. Eng. Sci.* **2020**, *157*, 103395. [[CrossRef](#)]
65. Kiani, K. Elastic waves in uniformly infinite-periodic jungles of single-walled carbon nanotubes under action of longitudinal magnetic fields. *J. Braz. Soc. Mech. Sci.* **2019**, *41*, 418. [[CrossRef](#)]
66. Ebrahimi, F.; Dehghan, M.; Seyfi, A. Eringen's nonlocal elasticity theory for wave propagation analysis of magneto-electro-elastic nanotubes. *Adv. Nano Res.* **2019**, *7*, 1.
67. Farajpour, M.R.; Shahidi, A.R.; Farajpour, A. Elastic waves in fluid-conveying carbon nanotubes under magneto-hygro-mechanical loads via a two-phase local/nonlocal mixture model. *Mater. Res. Exp.* **2019**, *6*, 0850a8. [[CrossRef](#)]
68. Selvamani, R.; Tornabene, F.; Baleanu, D. Two phase local/nonlocal thermo elastic waves in a graphene oxide composite nanobeam subjected to electrical potential. *Z. Angew. Math. Mech.* **2023**, *103*, e202100390. [[CrossRef](#)]
69. Su, Y.C.; Cho, T.Y. Wave propagation in an embedded single-walled carbon nanotube. *Mech. Adv. Mater. Struct.* **2023**, *30*, 2850–2862. [[CrossRef](#)]
70. Farhadipour, F.; Mamandi, A. Nonlocal wave propagation analysis of a rotating nanobeam on a Pasternak foundation. *J. Vib. Control* **2023**. [[CrossRef](#)]
71. Kiani, K. Magneto-thermo-elastic fields caused by an unsteady longitudinal magnetic field in a conducting nanowire accounting for eddy-current loss. *Mater. Chem. Phys.* **2012**, *136*, 589–598. [[CrossRef](#)]
72. Kiani, K. Nonlocal continuous models for forced vibration analysis of two- and three-dimensional ensembles of single-walled carbon nanotubes. *Physica E* **2014**, *60*, 229–245. [[CrossRef](#)]
73. Trabelssi, M.; El-Borgi, S.; Fernandes, R.; Ke, L.L. Nonlocal free and forced vibration of a graded Timoshenko nanobeam resting on a nonlinear elastic foundation. *Compos. Part B-Eng.* **2019**, *157*, 331–349. [[CrossRef](#)]
74. Zhao, X.; Wang, C.F.; Zhu, W.D.; Li, Y.H.; Wan, X.S. Coupled thermoelastic nonlocal forced vibration of an axially moving micro/nano-beam. *Int. J. Mech. Sci.* **2021**, *206*, 106600. [[CrossRef](#)]
75. Chen, B.; Lin, B.; Yang, Y.; Zhao, X.; Li, Y. Analytical solutions of nonlocal forced vibration of a functionally graded double-nanobeam system interconnected by a viscoelastic layer. *Z. Naturforsch. A* **2022**, *77*, 851–873. [[CrossRef](#)]
76. Kaghazian, A.; Hajnayeb, A.; Foruzande, H. Free vibration analysis of a piezoelectric nanobeam using nonlocal elasticity theory. *Struct. Eng. Mech.* **2017**, *61*, 617–624. [[CrossRef](#)]
77. Atanasov, M.S.; Stojanović, V. Nonlocal forced vibrations of rotating cantilever nano-beams. *Euro. J. Mech.-A Solids* **2020**, *79*, 103850. [[CrossRef](#)]
78. Hosseini, S.A.; Rahmani, O.; Bayat, S. Thermal effect on forced vibration analysis of FG nanobeam subjected to moving load by Laplace transform method. *Mech. Based Des. Struct.* **2023**, *51*, 3803–3822. [[CrossRef](#)]
79. Ma, X.; Kiani, K. Spatially nonlocal instability modeling of torsionally loaded nanobeams. *Eng. Anal. Bound. Elem.* **2023**, *154*, 29–46. [[CrossRef](#)]
80. Ma, X.; Sahmani, S.; Safaei, B. Quasi-3D large deflection nonlinear analysis of isogeometric FGM microplates with variable thickness via nonlocal stress-strain gradient elasticity. *Eng. Comput.* **2022**, *38*, 3691–3704. [[CrossRef](#)]
81. Karami, B.; Janghorban, M.; Rabczuk, T. Dynamics of two-dimensional functionally graded tapered Timoshenko nanobeam in thermal environment using nonlocal strain gradient theory. *Compos. Part B-Eng.* **2020**, *182*, 107622. [[CrossRef](#)]
82. Kiani, K.; Mehri, B. Assessment of nanotube structures under a moving nanoparticle using nonlocal beam theories. *J. Sound Vib.* **2010**, *329*, 2241–2264. [[CrossRef](#)]
83. Arani, A.G.; Roudbari, M.A. Nonlocal piezoelectric surface effect on the vibration of visco-Pasternak coupled boron nitride nanotube system under a moving nanoparticle. *Thin Solid Film.* **2013**, *542*, 232–241. [[CrossRef](#)]
84. Kiani, K.; Wang, Q. On the interaction of a single-walled carbon nanotube with a moving nanoparticle using nonlocal Rayleigh, Timoshenko, and higher-order beam theories. *Euro. J. Mech. A-Solids* **2012**, *31*, 179–202. [[CrossRef](#)]
85. Pourseifi, M.; Rahmani, O.; Hoseini, S.A. Active vibration control of nanotube structures under a moving nanoparticle based on the nonlocal continuum theories. *Meccanica* **2015**, *50*, 1351–1369. [[CrossRef](#)]
86. Kiani, K.; Roshan, M. Nonlocal dynamic response of double-nanotube-systems for delivery of lagged-inertial-nanoparticles. *Int. J. Mech. Sci.* **2019**, *152*, 576–595. [[CrossRef](#)]
87. Yu, G.; Kiani, K.; Roshan, M. Dynamic analysis of multiple-nanobeam-systems acted upon by multiple moving nanoparticles accounting for nonlocality, lag, and lateral inertia. *Appl. Math. Model.* **2022**, *108*, 326–354. [[CrossRef](#)]
88. Hashemian, M.; Falsafioon, M.; Pirmoradian, M.; Toghraie, D. Nonlocal dynamic stability analysis of a Timoshenko nanobeam subjected to a sequence of moving nanoparticles considering surface effects. *Mech. Mater.* **2020**, *148*, 103452. [[CrossRef](#)]
89. Roudbari, M.A.; Jorshari, T.D.; Arani, A.G.; Lü, C.; Rabczuk, T. Transient responses of two mutually interacting single-walled boron nitride nanotubes induced by a moving nanoparticle. *Eur. J. Mech. A-Solids* **2020**, *82*, 103978. [[CrossRef](#)]
90. Jorshari, T.D.; Roudbari, M.A.; Scerrato, D.; Kouzani, A. Vibration suppression of a boron nitride nanotube under a moving nanoparticle using a classical optimal control procedure. *Contin. Mech. Therm.* **2019**, *31*, 1825–1842. [[CrossRef](#)]
91. Rezapour, B.; Fariborzi Araghi, M.A.; Vázquez-Leal, H. Application of homotopy perturbation method for dynamic analysis of nanotubes delivering nanoparticles. *J. Vib. Control* **2021**, *27*, 802–814. [[CrossRef](#)]

92. Hosseini, S.A.; Khosravi, F.; Ghadiri, M. Effect of external moving torque on dynamic stability of carbon nanotube. *J. Nano Res.* **2020**, *61*, 118–135. [[CrossRef](#)]
93. Rezapour, B.; Fariborzi Araghi, M.A. Nanoparticle delivery through single walled carbon nanotube subjected to various boundary conditions. *Microsys. Technol.* **2019**, *25*, 1345–1356. [[CrossRef](#)]
94. Farajpour, M.R.; Shahidi, A.R.; Tabataba'i-Nasab, F.; Farajpour, A. Vibration of initially stressed carbon nanotubes under magneto-thermal environment for nanoparticle delivery via higher-order nonlocal strain gradient theory. *Eur. Phys. J. Plus.* **2018**, *133*, 1–5. [[CrossRef](#)]
95. Salamat, D.; Sedighi, H.M. The effect of small scale on the vibrational behavior of single-walled carbon nanotubes with a moving nanoparticle. *J. Appl. Comp. Mech.* **2017**, *3*, 208–217.
96. Pirmoradian, M.; Torkan, E.; Toghraie, D. Study on size-dependent vibration and stability of DWCNTs subjected to moving nanoparticles and embedded on two-parameter foundations. *Mech. Mater.* **2020**, *142*, 103279. [[CrossRef](#)]
97. Kiani, K. Nonlocal continuum-based modeling of a nanoplate subjected to a moving nanoparticle. Part I: Theoretical formulations. *Physica E* **2011**, *44*, 229–248. [[CrossRef](#)]
98. Pouresmaeeli, S.; Fazelzadeh, S.A.; Ghavanloo, E. Exact solution for nonlocal vibration of double-orthotropic nanoplates embedded in elastic medium. *Compos. Part B-Eng.* **2012**, *43*, 3384–3390. [[CrossRef](#)]
99. Arani, A.G.; Kolahchi, R.; Gharbi Afshar, H. Dynamic analysis of embedded PVDF nanoplate subjected to a moving nanoparticle on an arbitrary elliptical path. *J. Braz. Soc. Mech. Sci.* **2015**, *37*, 973–986. [[CrossRef](#)]
100. Khaniki, H.B.; Hosseini-Hashemi, S. Dynamic response of biaxially loaded double-layer viscoelastic orthotropic nanoplate system under a moving nanoparticle. *Int. J. Eng. Sci.* **2017**, *115*, 51–72. [[CrossRef](#)]
101. Pirmoradian, M.; Torkan, E.; Abdali, N.; Hashemian, M.; Toghraie, D. Thermo-mechanical stability of single-layered graphene sheets embedded in an elastic medium under action of a moving nanoparticle. *Mech. Mater.* **2020**, *141*, 103248. [[CrossRef](#)]
102. Ejabati, S.M.; Fallah, N. Aerodynamic analysis of temperature-dependent FG-WCNTRC nanoplates under a moving nanoparticle using meshfree finite volume method. *Eng. Anal. Bound. Elem.* **2022**, *134*, 510–531. [[CrossRef](#)]
103. Kiani, K. Nonlocal excitation and potential instability of embedded slender and stocky single-walled carbon nanotubes under harmonically vibrated matrix. *Physica B* **2017**, *519*, 26–38. [[CrossRef](#)]
104. Nikkhoo, A.; Hassanabadi, M.E.; Azam, S.E.; Amiri, J.V. Vibration of a thin rectangular plate subjected to series of moving inertial loads. *Mech. Res. Commun.* **2014**, *55*, 105–113. [[CrossRef](#)]
105. Nikkhoo, A.; Farazandeh, A.; Ebrahimzadeh Hassanabadi, M.; Mariani, S. Simplified modeling of beam vibrations induced by a moving mass by regression analysis. *Acta Mech.* **2015**, *226*, 2147–2157. [[CrossRef](#)]
106. Ahmadi, M.; Nikkhoo, A. Utilization of characteristic polynomials in vibration analysis of non-uniform beams under a moving mass excitation. *Appl. Math. Model.* **2014**, *38*, 2130–2140. [[CrossRef](#)]
107. Kiani, K.; Nikkhoo, A.; Mehri, B. Assessing dynamic response of multispan viscoelastic thin beams under a moving mass via generalized moving least square method. *Acta Mech. Sin.* **2010**, *26*, 721–733. [[CrossRef](#)]
108. Şimşek, M. Vibration analysis of a single-walled carbon nanotube under action of a moving harmonic load based on nonlocal elasticity theory. *Physica E* **2010**, *43*, 182–191. [[CrossRef](#)]
109. Zhao, S.; Zhang, Y.; Zhang, Y.; Yang, J.; Kitipornchai, S. Vibrational characteristics of functionally graded graphene origami-enabled auxetic metamaterial beams based on machine learning assisted models. *Aerosp. Sci. Technol.* **2022**, *130*, 107906. [[CrossRef](#)]
110. Gutub, A. Boosting image watermarking authenticity spreading secrecy from counting-based secretsharing. *CAAI Trans. Intell. Technol.* **2022**, *8*, 1–13.
111. Hu, X.; Kuang, Q.; Cai, Q.; Xue, Y.; Zhou, W.; Li, Y. A Coherent pattern mining algorithm based on all contiguous column bicluster. *J. Artif. Intell. Technol.* **2022**, *2*, 80–92. [[CrossRef](#)]
112. Avci, O.; Abdeljaber, O.; Kiranyaz, S.; Hussein, M.; Gabbouj, M.; Inman, D.J. A review of vibration-based damage detection in civil structures: From traditional methods to Machine Learning and Deep Learning applications. *Mech. Syst. Signal. Process.* **2021**, *147*, 107077. [[CrossRef](#)]
113. Zhang, Z.; De Luca, G.; Archambault, B.; Chavez, J.; Rice, B. Traffic dataset and dynamic routing algorithm in traffic simulation. *J. Artif. Intell. Technol.* **2022**, *2*, 111–122. [[CrossRef](#)]
114. Li, Z.; Li, S. Recursive recurrent neural network: A novel model for manipulator control with different levels of physical constraints. *CAAI Trans. Intell. Technol.* **2023**, *8*, 622–634. [[CrossRef](#)]
115. Jackson-Mills, G.; Barber, A.R.; Blight, A.; Pickering, A.; Boyle, J.H.; Kaddouh, B.; Richardson, R.C. Non-Assembly Walking Mechanism Utilizing a Hexapod Gait. *J. Artif. Intell. Technol.* **2022**, *2*, 158–163.

**Disclaimer/Publisher's Note:** The statements, opinions and data contained in all publications are solely those of the individual author(s) and contributor(s) and not of MDPI and/or the editor(s). MDPI and/or the editor(s) disclaim responsibility for any injury to people or property resulting from any ideas, methods, instructions or products referred to in the content.